

NASW-4435 IV-05 KC


NASA ADVANCED DESIGN PROGRAM
ANALYSIS, DESIGN, AND CONSTRUCTION
OF A SOLAR POWERED AIRCRAFT

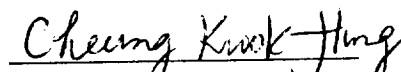
141621
P. 112

A Major Qualifying Project
Submitted to the Faculty
of the

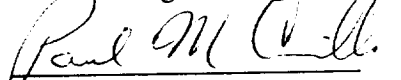
WORCESTER POLYTECHNIC INSTITUTE


in Partial Fulfillment of the Requirements
for the
Degree of Bachelor of Science
Submitted on May 5, 1992
by

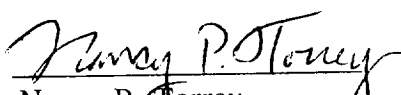

Agnes Chan

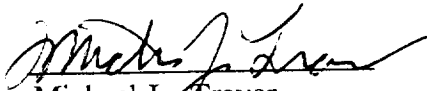

Kwok-Hung Cheung


Kristin Conley



Paul M. Crivelli

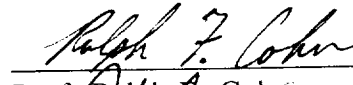

Christian T. Javorski

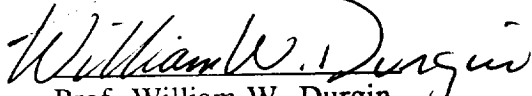

Nancy P. Torrey

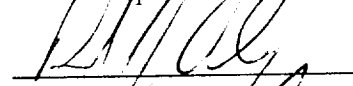

Michael L. Traver

Approved By:


Prof. Andreas N. Alexandrou


Prof. Ralph F. Cohn


Prof. William W. Durgin


Prof. David J. Ohinger

(NASA-CR-192040) NASA ADVANCED
DESIGN PROGRAM: ANALYSIS, DESIGN,
AND CONSTRUCTION OF A SOLAR POWERED
AIRCRAFT B.S. Thesis (Worcester
Polytechnic Inst.) 112 p

N93-17802

Unclass

ACKNOWLEDGEMENTS

The members of the project group would like to offer their gratitude to the following people for their support and guidance during the project:

Professor Andreas Alexandrou

Professor William Durgin

Professor Ralph Cohn

Professor David Olinger

Professor Edward Clarke

Kurt Heinzmann

Charlotte Cody

Adam Szymkiewicz

Arthur Lavalley of Mild to Wild Hobby Shop

Mr. Eric Tornstrom of Mobil Solar

NASA/USRA

Mobil Solar

Timothy Johnson

Todd Billings

Bob Taylor

Roger Steele

ABSTRACT

Increase in energy demands coupled with rapid depletion of natural energy resources have deemed solar energy as the most logical alternative source of power. The major objective of this project was to build a solar powered remotely controlled aircraft to demonstrate the feasibility of solar energy as an effective, alternate source of power. The final design was optimized for minimum weight and maximum strength of the structure. These design constraints necessitated a carbon fiber composite structure. *Surya* is a lightweight, durable aircraft capable of achieving level flight powered entirely by solar cells.

SOLAR POWERED MULTI-PURPOSE REMOTELY POWERED AIRCRAFT

Worcester Polytechnic Institute
Mechanical Engineering Department
Worcester, MA

Dr. A. N. Alexandrou, Dr. W. W. Durgin, Dr. R. F. Cohn, Dr. D. J. Olinger
Charlotte K. Cody, Teaching Assistant
Agnes Chan, Kwok-Hung Cheung, Kristin Conley, Paul M. Crivelli, Christian T. Javorski,
Nancy P. Torrey, Michael L. Traver

ABSTRACT

Increase in energy demands coupled with rapid depletion of natural energy resources have deemed solar energy as an attractive alternative source of power. The focus of this work was to design and construct a solar powered, remotely piloted vehicle to demonstrate the feasibility of solar energy as an effective, alternate source of power. The final design included minimizing of the power requirements and maximizing of the strength-to-weight and lift-to-drag ratios. Given the design constraints, *Surya* (the code-name given to the aircraft), is a lightweight aircraft primarily built using composite materials and capable of achieving level flight powered entirely by solar energy.

INTRODUCTION

Mission Requirements

As civilization enters the 21st century, considerations for alternative energy sources are becoming necessary. Natural energy sources such as coal, oil, and fossil fuels are quickly depleting. In addition, they are harmful to the environment. Their use has caused a substantial increase in air pollution, and they have thus been major contributors to the greenhouse effect. Although nuclear energy is immediately available, high operational risks and environmental issues have made it a questionable option. Solar energy is not only pollution free, but it is also available in abundance. Proper utilization of the sun's energy can result in an inexpensive and effective power source. One of the main objectives of this project was to demonstrate the effectiveness and feasibility of using solar energy to power an airborne vehicle. The final configuration of the solar plane was optimized for minimum level flight power.

Aircraft Configuration

The proposed vehicle is shown in Figures 1 and 2. General data and design parameters are summarized in Table 1.

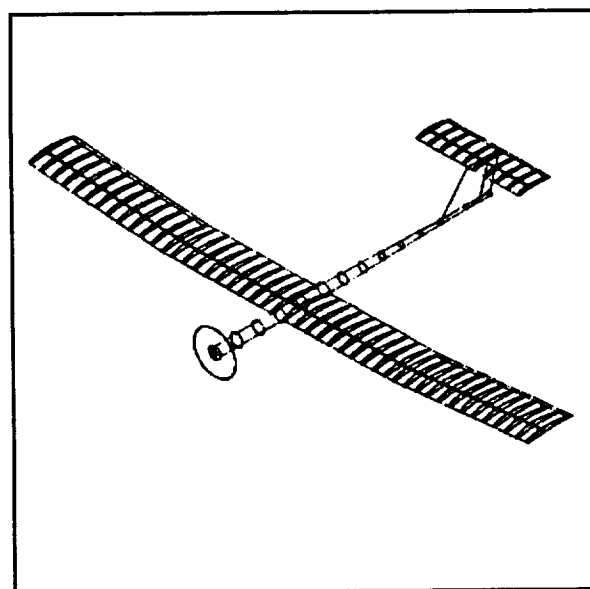


Figure 1: *Surya* Isometric View

Table 1: General Data

Weight	W_{gross}	40 N
Wing Area	S	1.48 m ²
Wing Loading	W	27.03 N/m ²
Aspect Ratio	AR	8.25
Wingspan	b	3.5 m
Cruise Altitude	h	50 m
Cruise Velocity	V	7 m/s
Design Lift Coeff	C_L	0.83
Design Lift-to-Drag	L/D	15.75
Cruise Power Req'd	P	15.9 W
Design Load Factor	n	7

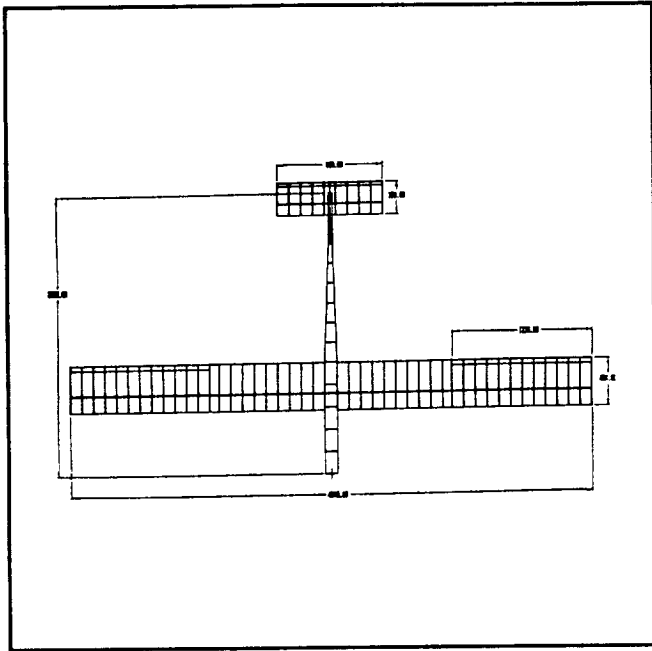


Figure 2: *Surya* Top View

The wing has a span of 4.5 m, a chord length of 42.4 cm, an aspect ratio of 10.61, and is positioned at a geometric attack angle of 4 degrees. A lift coefficient of 0.8274 is generated by the wing during level flight. The tail is oriented at an angle of attack of 0 degrees and its lift coefficient is 0.4053. The tail efficiency is assumed to be 0.85.¹ The overall configuration has a total lift coefficient of 0.8816, a total drag coefficient of 0.0451, yielding a L/D ratio of 19.548.

The wing design includes a dihedral of 2.5 degrees. The vertical stabilizer has an effective area of 900 cm², the rear half being the rudder. Situated 1.6 meters behind the aerodynamic center of the wing, the horizontal stabilizer spans one meter and is composed of a NACA 6409 airfoil with a 30 cm chord. The rear quarter of this chord is a hinged flap which serves as the elevator. The ailerons are located on the modular wing sections, occupying the aft 12% of the chord and spanning the entire length. To ensure pitch stability and optimum lift for the plane as a whole, the center of gravity is maintained a tenth of the wing's chord behind its aerodynamic center. The location of the electronics harness in the nose of the fuselage is adjustable and can be moved either forward or backward to insure the center of gravity is positioned to maintain static stability.

A total of 120 solar cells are contained within the wing of *Surya*. This number was determined through required power estimations. Conservative estimates predicted about 100 watts for the array output at any given time during flight. Although this number is rather high, the actual amount of power delivered to the motor and propeller was

much less. On an open circuit, the cells developed a potential of 5.8 volts while producing approximately 19 amps of current when short circuited. As load is applied to the array, these values drop to 4.7 volts and between 12 and 14 amps. To produce the required power, 12 arrays containing 10 cells were constructed. The five volt potential is the result of the 10 cells wired in series with each individual cell producing 0.5 volts. The 12 amp current is generated by wiring the 12 sub-arrays in parallel at 1 amp each.

The solar array is split into three rows per wing section. The leading edge row is placed underneath the skin to preserve the integrity of the front part of the airfoil, where it is most crucial. The trailing rows adhere directly to the skin on the outside of the wing to increase power production. The first row sits at an angle of 12° with respect to the chord while the back rows sit at an angle of 6°. As a result, optimum power is produced by the array during level flight with the plane flying directly away from the sun.

Surya's total coefficient of lift was estimated at 0.88, and both the tail and the wing act as lifting surfaces. With a weight of 52 N and an estimated parasitic drag coefficient at 0.148, the plane is expected to have a minimum flight speed of 7.1 m/s and a minimum required power to achieve this speed of 18.8 Watts.

The climb capability of the plane is strictly determined by the amount of excess power available. *Surya*'s climb rates vary depending on the output of power from the solar cells at that time interval, and the position of the plane relative to the sun.

Banking and turning is another basic maneuver at which the plane must remain in level flight. Since the flight velocity of the solar plane is low, the banking angles are small. With small banking angles between 3 and 4 degrees, the turn radii necessary are 89 and 67 m respectively. Hence, the proposed spiral climb scheme for the 50 m altitude climb can be accomplished in about five minutes within a 200 m length field.

DESIGN AND ANALYSIS

Aircraft Sizing and Weight Estimation

Preliminary component sizing was dictated by set parameters such as the chosen airfoil, the size of the solar cells, and the desired lift-to-drag ratio. The optimization of the design included the minimization of the power requirements and the maximization of the strength-to-weight and lift-to-drag ratios. The resulting configuration has a wing span of 4.5 m, a tail span of 1 m, and a fuselage length of 2.5 m. Due to the large span, the wing was constructed in modular sections for storage purposes. Tables 2 through 4 break down the masses of individual

Table 2: Wing Component Masses

WING	Mass (g)	% Wing
Carbon Composite Spars	478.0	15.9
Ribs	132.0	4.4
Leading Edge	116.0	3.8
Trailing Edge	58.0	1.9
Ailerons	99.0	3.3
Spar Webs	44.8	1.5
Skin (Mylar)	254.4	8.4
Wing Tips	36.1	1.2
Solar Cells	1142.0	37.9
Servos	43.0	1.4
Wiring	148.0	4.9
Reinforced Rib	158.0	5.3
Modular Tube Connection	107.0	3.6
Landing Gear	58.0	1.9
Misc.	139.0	4.6
TOTAL	3013.4	100

elements of the plane showing their percent contribution to each section of the aircraft.

Aerodynamic Design and Analysis

The wing has a rectangular platform with a wing span of 4.5 m and a chordlength of 0.424 m. The aspect ratio of the wing is 10.61 and the geometrical angle of attack is 4°. The wing generates a lift coefficient, C_L , of 0.8274 at level flight conditions. The tail has a rectangular platform, a tail span of 1 m, and a chordlength of 0.3 m. The resulting aspect ratio of the tail is 3.333. At level flight conditions, the geometrical angle of attack of the tail is 0° and the C_L is 0.4053. The tail efficiency was assumed to be 0.85.² With this configuration, the aircraft has a total lift coefficient of 0.8816 and a total drag coefficient of 0.0451. As a result, the total lift to drag ratio is equal to 19.548.

The chord Reynolds number is relatively low since a solar aircraft has a fairly slow cruise velocity. Theoretically, viscous effects dominate the flow at low Reynolds numbers, thus resulting in flow separation and a laminar separation bubble. However, at Reynolds number of 200,000 or

Table 3: Fuselage Component Masses

FUSELAGE	Mass (g)	% Fuse
Carbon Composite Frame	900.0	48.9
Servo	21.5	1.2
Wiring	98.3	5.3
Motor	245.7	13.3
Nose Cone	56.8	3.1
Propeller	42.9	2.3
Receiver Battery	101.1	5.5
Receiver	44.0	2.4
On/Off Switch	63.3	3.4
Emergency Batteries	238.0	12.9
Miscellaneous	32.0	1.7
TOTAL	1843.5	100

Table 4: Tail Component Masses

TAIL	Mass (g)	% Tail
Ribs	14.8	3.3
Leading Edge	25.8	5.7
Spar Webs	6.4	1.4
Elevator	43.9	9.7
Skin (Mylar)	47.3	10.5
Carbon Spar	59.0	13.0
Vertical Tail	160.0	35.4
Servos	43.0	9.5
Balsa Rudder	12.0	2.7
Miscellaneous	40.0	8.8
TOTAL	452.2	100

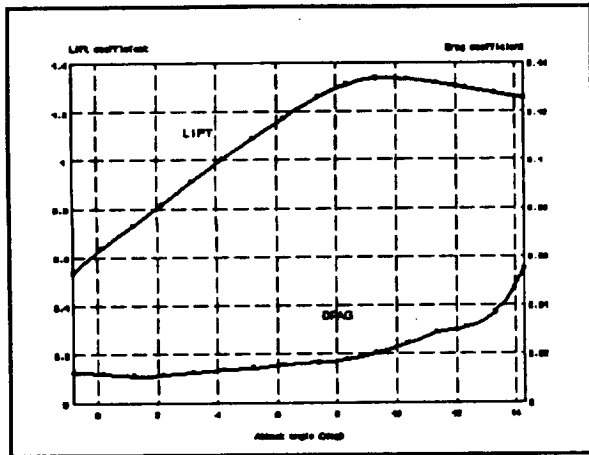


Figure 3: Sectional Lift and Drag Coefficients

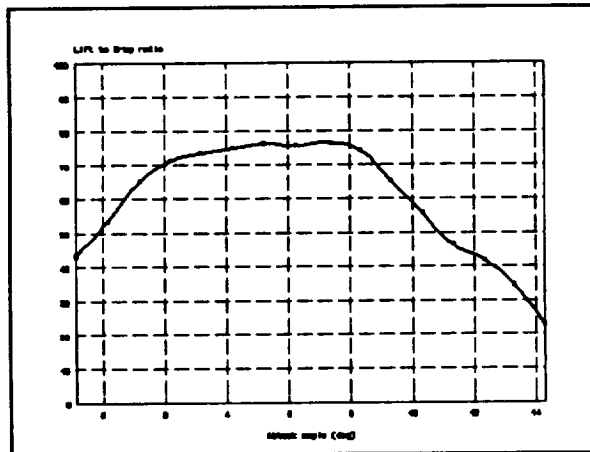


Figure 4: Sectional Lift-to-Drag Ratio

higher, a turbulent boundary layer develops and gives more resistance to flow separation during the pressure recovery. For this reason, it was decided to operate the plane at a Reynolds number based on the chord of about 200,000. In addition, the effects of compressibility are neglected in the entire aerodynamic analysis, since the Mach number during level flight is much less than 0.3.

The NACA 6409 was chosen as the airfoil section for the wing and the tail. It has a 9% maximum thickness and a 6% maximum chamber at a distance of 40% of the chord from the leading edge. Figure 3 shows the experimental lift and drag characteristic of the NACA 6409 airfoil at the Reynolds number of 200,100.³ The sectional lift curve slope of the airfoil is about 5.17 per radian between an angle of attack of -0.87 and 7.32 degrees. At an angle of attack of 9.32 degrees, the sectional lift coefficient reaches a maximum value of 1.342. Meanwhile, the sectional drag coefficient varies parabolically and has a minimum drag coefficient of 0.0112 at an angle of attack of 1.20 degrees.

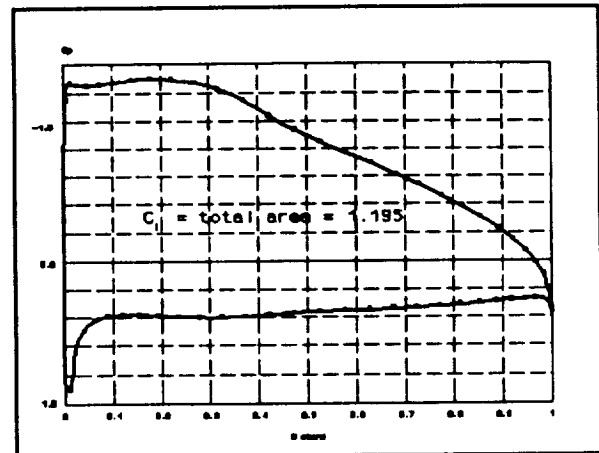


Figure 5: Inviscid Pressure Distribution

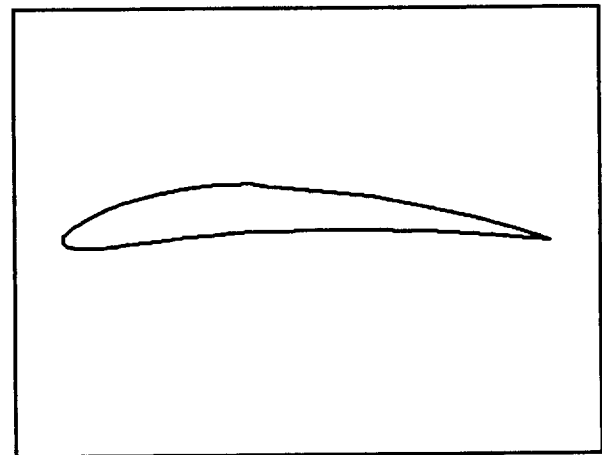


Figure 6: Modified NACA 6409 With Flattened Back

The lift to drag ratio of the airfoil is calculated and summarized in Figure 4. As shown in the figure, the airfoil provides a constant high lift to drag ratio between the angles of attack of 2 and 8 degrees and therefore allows for a wide range of favorable operating conditions.

In order to increase the power generated by the solar propulsion system, cells are placed on the surface of the wing. Since the solar cells are flat and not flexible, the shape of the airfoil is slightly changed. As a result, the sectional characteristics of the airfoil are affected. By using the vortex panel method⁴, the inviscid pressure distribution of the original NACA 6409 was calculated as shown in Figure 5. In the figure, it is clearly shown that the majority of the lift is generated in the front 40% of the airfoil. Therefore, in order to minimize the aerodynamic effects due to the solar cells placement, the cells were placed behind a distance of 40% of the chord from the leading edge, see Figure 6. The inviscid pressure distribution of the airfoil which has the solar cells on the back is shown in Figure 7.

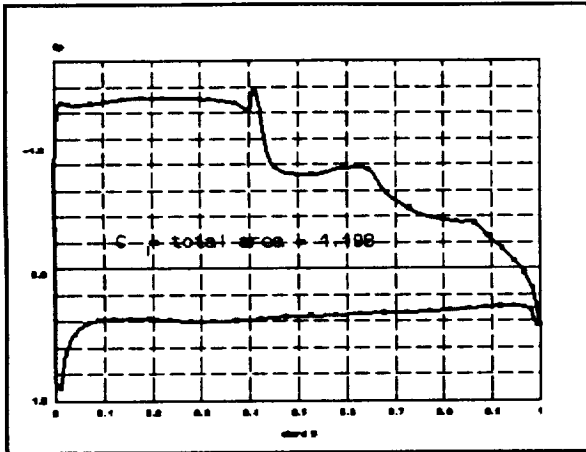


Figure 7: Inviscid Pressure Distribution for Modified NACA 6409

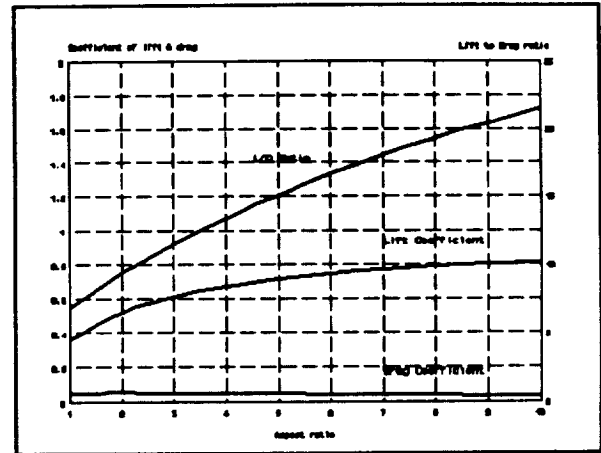


Figure 9: Effects of the Aspect Ratio on Lift & Drag

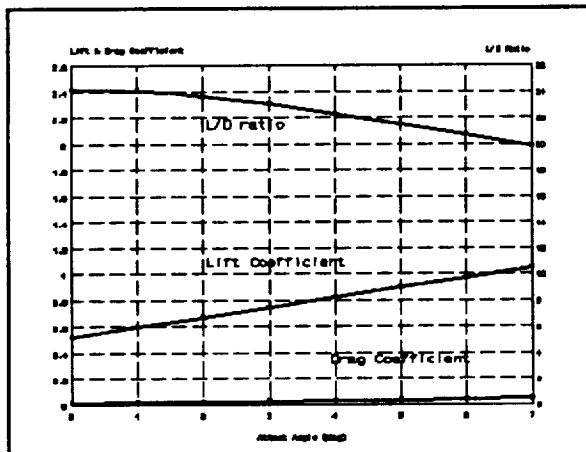


Figure 8: Lift & Drag Characteristics of the Finite Wing

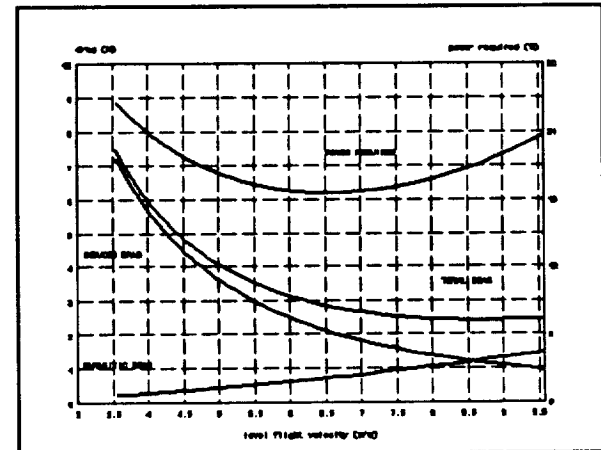


Figure 10: Power Required vs Flight Velocity

At an angle of attack of 4° , the difference between the inviscid lift coefficients of the original airfoil and the one which has solar cells on the back is only about 0.25 %.

Assuming the flow does not separate before the first 40% of the chord, the aerodynamic characteristics of the modified airfoil are apparently similar to the original NACA 6409. Therefore, the experimental data of the NACA 6409 airfoil are assumed to be valid for the design

Using the Glauert Method and the modified flat plate theory⁵, the finite lift and drag coefficients of the wing and tail are determined. Figure 8 shows the finite lift and drag characteristic of the wing at different attack angles. In addition, the aspect ratio effects to the L/D ratio are investigated. With a higher aspect ratio, the wing behaves closer to the predicted performance of the airfoil section. As a result, the wing generates more lift and experiences less induced drag. In Figure 9, it shows clearly that the lift to drag ratio increases while the aspect ratio of the wing

increases.

The power required for level flight at different velocities is summarized in Figure 10. As the figure shows, the optimum level flight speed is 6.388 m/s and the corresponding attack angle is 6.77 degrees. At this condition, the power required for level flight is equal to 18.682 Watts. Due to safety considerations, it was decided to operate at an attack angle of 4° , with the corresponding cruising speed is 7.104 m/s. The required power is 18.839 Watts and which is 0.84% higher than the power required at the optimum condition.

Structural Design and Analysis

The main supporting structure of the wing is a rigid tube running the length of the span, effectively acting as a wing spar. The outer diameter of the tube was limited by the thickness of the airfoil. The thickness of the tube was determined by a simplified stress analysis of the

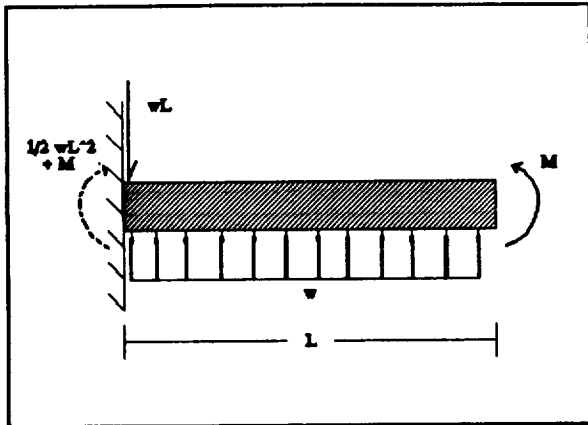


Figure 11: Wing Loading Model

loads applied to the spar.

A simplified half wing loading model was developed to estimate the maximum stress on the wing spar, see Figure 11. The carbon spar was to assume all of the loads due to the lift generated. The wing was modeled as a cantilevered beam with a distributed load, and a moment load applied at the free end. The lift of 48.3 Newtons was represented by a distributed load of 10.73 N/m acting along the full span. This load produces an effective moment of 5.36 N-m located at the connection point, shown at the free end of the beam. These calculations were adjusted to account for the potential gust load the wing may endure. With a gust load factor of 3, the loads were increased to a distributed load of 32.19 N/m and an effective moment of 16.09 N-m.

The shear and moment distributions of the wing are illustrated in Figure 12. The locations of maximum shear and maximum bending moment were determined from these diagrams, 40.24 N and 41.24 N-m respectively. The maximum normal stress resulting from expected loads and the material properties of carbon fiber were considered, shear stress was determined to be negligible in comparison. Carbon composite spars were constructed and tested to obtain accurate material properties. Considering the maximum expected load and a safety factor of 1.2, the maximum allowable stress for the spar was calculated and determined to be $2.75E+8$ N/m². The minimum required spar thickness was iteratively determined. A wing spar having an outer diameter of 20.1 mm, 0.53 mm thickness (3 layers of fabric), and capable of withstanding a maximum load of $3.303E+8$ N/m² was constructed. The tail was modeled and analyzed similarly to that of the wing, differing only by the absence of a moment at the free end. The lift on the tail was calculated to be 3.7 Newtons and a distributed load of 3.7 N/m was modeled. The resulting tail spar dimensions are an outer diameter of 1.38 cm and a thickness of 0.53 mm. The sizing of the fuselage was dependent on the placement of the tail and the area required to house the electronics and was determined to be 2.5

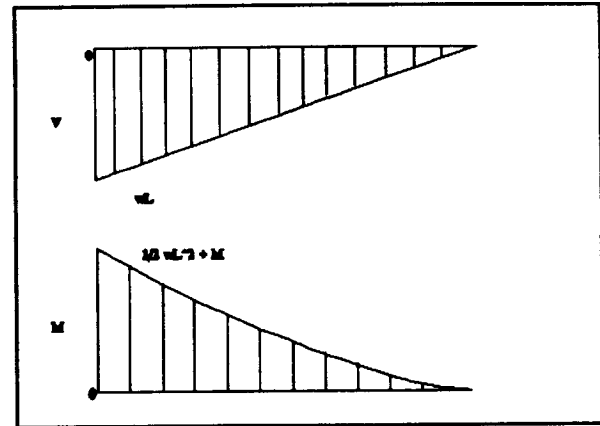


Figure 12: Shear & Moment Diagrams

meters. The anterior portion of the fuselage is 10.5 cm in diameter, which was determined by an estimation of the size of the electronic components. This diameter gradually decreased with length in order to minimize weight. The posterior segment has a diameter of 3 cm. This value was determined to be the minimum within the margin of safety. The required thickness of the fuselage wall for this design was 0.36 mm (2 fabric layers).

Material Selection

The material selection process played a key role in the design. Since the limited power available from the solar cells mandated weight minimization, effective material selection was crucial in the design process. While the weight of the structure needed to be minimized, a high strength material was desired to withstand the applied loads. This dictated the use of composite materials because they exhibit a high strength to weight ratio.

Many composite fabrics were tested including carbon, kevlar, and fiberglass. Carbon was selected due to its high strength-to-weight ratio and inherent rigidity. Consequently, the wing spar, tail spar, and fuselage were constructed using this material. Furthermore, a number of different spar configurations were tested to determine the material constraints at different loads. These tests led to the selection of a hollow circular cross-section. Sample hollow rod configurations were tested to determine the thickness of the tube required to withstand the expected stress.

The vertical stabilizer which supports the tail spar was constructed using a foam structure which was reinforced with carbon composite fabric on both sides. The carbon composite provided the strength needed to support the tail and foam was used as a spacer.

Since the wing spar was modular, a connecting support was used to form the dihedral angle in the wing and withstand the load applied at the connection. The modular connection supports utilized a foam and carbon composite combination much like that of the vertical stabilizer with

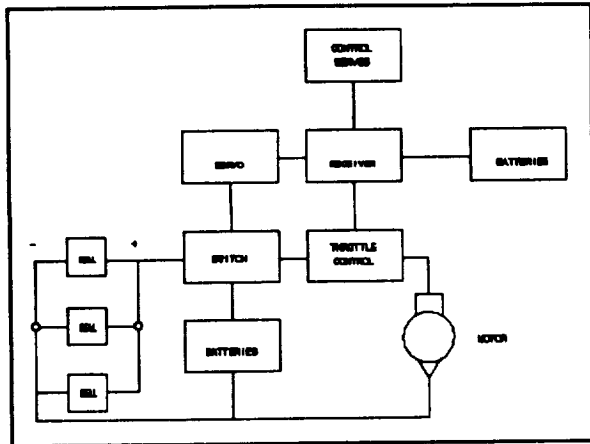


Figure 13: Controls Layout

foam sandwiched between two layers of carbon composite fabric. Foam was used as a spacer in the vertical stabilizer and modular connection supports because of its low density making it the most lightweight material used in the plane. The carbon composite fiber and foam combination proved to be ideal when used on components that were designed to withstand pure bending loads. Foam was used to construct components without structural applied loads, such as the solar cell braces, nose cone, and wing tips.

Balsa wood was utilized for many components that sustained small loads and required a precise shape. Since balsa is the lightest of all wood and very easily shaped it was favored over foam. Balsa wood was used for components such as the ribs, the leading and trailing edges, the ailerons, the elevator, and the horizontal stabilizer. The ailerons and the horizontal stabilizer utilized balsa wood in a truss structure designed as an extension of the airfoil.

Heat shrinking mylar was used for vehicle's skin. It was necessary to use a material with a high transmissivity on the top of the wing allowing the sunlight to reach the solar cells underneath the skin, but at the same time the material had to be strong enough to sustain the shape of the airfoil it formed. Another concern about the material of the skin was a desired resistance to tear as deformation of the wing was experienced. Mylar becomes rigid after being heat shrunk over a surface but it remains adequately flexible enough to deform.

Propulsion System Design and Integration

The modified remote control radio system and the necessary hardware for controlling deflecting surfaces and switches via servo-motor, shown in Figure 13, is the essence of the controls and interface scheme.

The Astro Cobalt 05 electric, geared motor and a two-bladed, folding propeller with a diameter of 33 cm and pitch of 16.5 cm manufactured by Aero-Haute were chosen for their combined efficiency. A combined contour plot of

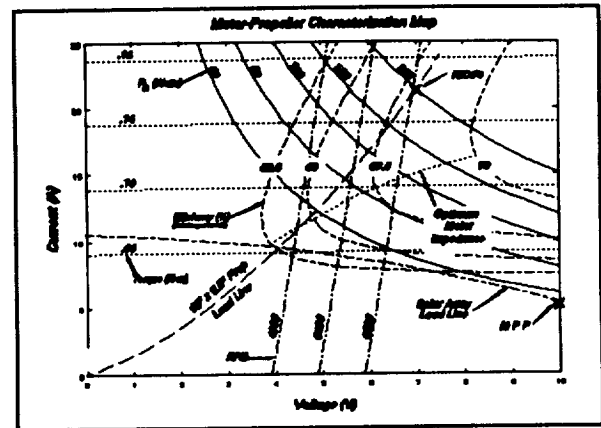


Figure 14: Combined Contour Plot for Design Motor-Propeller

electrical input power, shaft torque, shaft RPM, and motor efficiency versus voltage and current is shown in Figure 14. Several motor-propeller combinations were tested in the WPI wind tunnel under conditions similar to those in flight. Figure 15 illustrates the results of the tests performed for the chosen motor-propeller combination.

As a safety feature, there is a NiCad battery pack installed in the fuselage of the plane. At full power they produce eight to nine volts and upwards of 20 amps. The use of these batteries is limited as their lifespan is not more than five or six minutes. A manual switch shifts the power source from the cells to the batteries. The batteries can be slowly recharged up to five volts during glides if the motor is turned off. A diode connected between the cells and the batteries prevents the batteries from charging the array.

The control surfaces are operated by remote control through the use of the servos. A very small current is needed to run each servo is controlled by its own channel frequency. Both ailerons are wired into the same channel to act in opposite directions. The rudder and the horizontal stabilizer are wired separately and receive their own channels. All servos are wired to the receiver box where they pick up the signals for operation. The receiver itself needs a small battery pack to operate. These are four rechargeable 1.2 volt cells. There are enough channels available on the receiver to not only handle the control surfaces, but also the throttle and the main power switch.

The power requirements for level flight are met through the utilization of silicon solar cells. The level flight speed of 7.1 m/s and the weight of 52 Newtons dictate a minimum power requirement of 18.8 Watts. The solar array implemented on the plane produces approximately 108 Watts for the test flight date (April 11, 1992). This power production is calculated with the plane flying away from the sun thus exposing the greatest cell area to the sun's rays. The power produced for the plane flying toward the sun is approximately 98 Watts. These values do not include the

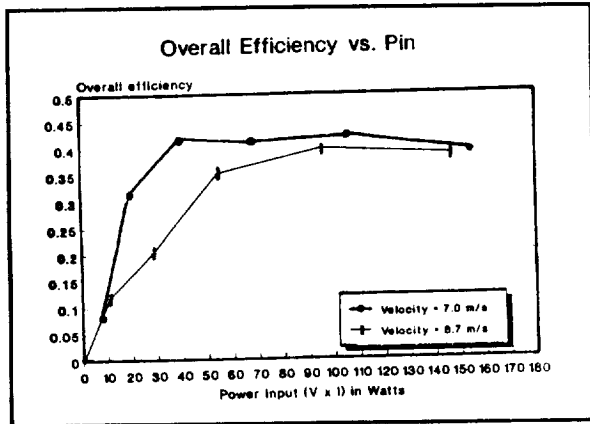


Figure 15: Efficiency vs Power Input for Design Motor-Propeller

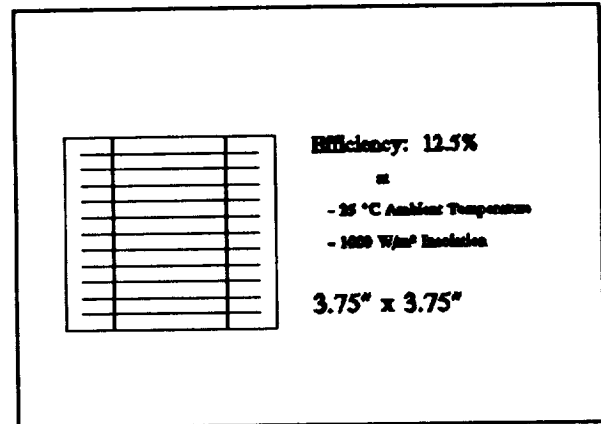


Figure 16: Mobil Solar Silicon Photovoltaic Cell.

power losses suffered in the motor/propeller transmission since even an optimized power train reduces the power by more than half.

A number of parameters control the amount of power produced as well as the construction of the array. The weight of the cells are considerable and compose a large portion of the overall weight of the plane. Therefore, the cells must produce more power to the overall thrust than they contribute to weight. The photovoltaic cells are rated at an efficiency of 12.5%, determined at ideal conditions in a laboratory. The actual efficiency is lower due to design conditions. Substantial power loss occur due to impedance matching and resistance of the wiring. The wing geometry allows only a limited number of possible array configurations and limits the number of possible voltage-current options.

A basic solar cell, see Figure 16, consists of two layers of Silicon glass. The top layer is doped with Phosphorous to produce an excess of electrons while the bottom layer is doped with Aluminum to produce an abundance of electron holes. As photons strike the surface of the cell, they knock loose the excess electrons in the SiP bond. The net effect is the creation of free conduction electrons and positively charged holes which generate an electric potential between the top and bottom layers. Basic inefficiencies in this process are reflection and recombination of the photons striking the cell. Also, some photons do not possess the energy to knock loose the electrons thus rendering some of the incident light ineffective. Other photons possess too much energy and waste the excess when striking the electrons.⁶

The amount of solar power reaching the cells on a given day relies on many geometric and atmospheric variables. Obviously, a clear sunny day is better than an overcast day, yet summer months are not necessarily better than winter. Air pollution and building reflection contribute to the decrease in power availability. However, the position of the

sun relative to the cells is the dominating factor.

The power received is not the available energy, since the cells can only convert around 12.5% to electric power. This electric power is eventually transformed into thrust through the motor and propeller configuration. Therefore, the cells must produce enough power to overcome the losses induced by the power train to sustain level flight. Assuming that the power train will convert only about 20 to 30 %, this target and the estimated power produced dictate the initial number of cells to be installed upon the plane. With 18.8 Watts needed to fly the plane and the wing geometry in mind, the number of cells to be placed upon the wings is 120.

A random sampling of solar cells were taken to the roof of Salisbury Laboratories on the 18th of November 1991, and tested for their open circuit voltage and short circuit current. On that day, the individual cells produced approximately 0.5 Volts and, depending upon the orientation, 0.6 - 1.1 Amps. A similar test was performed on February 6, 1992. This test used a ten cell array and the characteristic I-V curve and maximum power point for the array were determined, see Figures 17 and 18. The clear mylar skin array reduces the amount of current produced, thus affecting the power available. For this reason, as many cells as possible were placed on the outside of the wing to maximize power production. Each array on the plane must have an equal number of cells, avoiding losses due to internal circuits.

The array was configured to accommodate the desired wing geometry and the predicted load. The chord of the wing allows for the placement of three rows of cells along the entire span. In order to maintain the desired aerodynamic characteristics of the aircraft the first row on the leading edge is placed underneath the wing skin. The second and third rows are placed on the outside of the wing on the rear of the airfoil. The arrays should be angled to receive the greatest amount of sunlight at any given time.

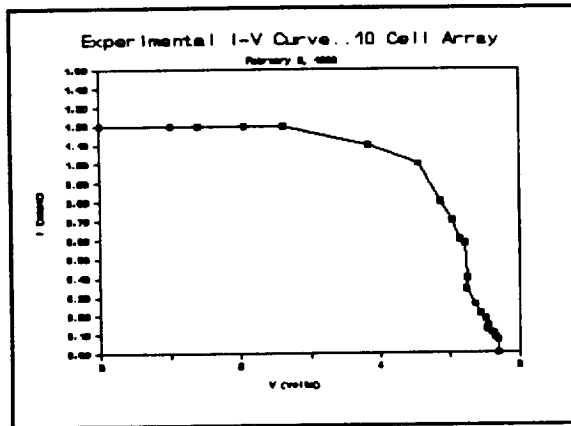


Figure 17: Experimentally Determined I-V Curve

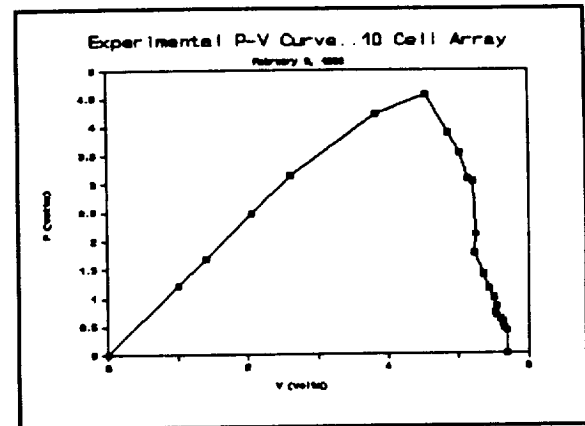


Figure 18: Experimentally Determined P-V Curve

On a stationary platform the array would be angled at about 45° to the horizontal. Since the plane is constantly moving in the horizontal and vertical planes, the best inclination is to place them close to the horizontal. The front cells are inside facing forward and placed as close to horizontal as the wing geometry will allow at an angle of 12° to the chordline. The rear cells are subject to geometric constraints as well and are placed directly onto the flatback airfoil at angles of approximately 6° to the chordline.

The constructed array consists of twelve sub-arrays of ten cells placed on both the main and modular sections of the wing and integrated into the propulsion system. All twelve are connected in parallel to generate an anticipated 5 Volts and 12 Amps.

Construction Process

The wing and tail supporting spars and the tapered fuselage were uniquely constructed using a woven carbon fabric and West System epoxy to create durable, lightweight components. A piece of ordinary PVC wrapped in mylar to prevent any adhesion to the resultant carbon tube, served as a mold for the spars. The fuselage mold was constructed using PVC tubing of the desired diameters with a tapered section made of foam connecting them. Wrapping the carbon fabric about the molds and applying epoxy generated components with desirable strength-to-weight characteristics. A microlyte filler was applied to the finished carbon structure to smooth out the imperfections and reduce the drag on this member. The main wing was connected to the fuselage by drilling a hole through the fuselage and passing the wing tube through the center of the body. The connection was reinforced using carbon fiber sleeves. Subsequent tasks included gluing the ribs to the wing spar, applying the mylar, and wiring all of the electrical components and solar cells.

The solar cell array was connected entirely by hand.

Each of the 120 cells donated by Mobil Solar arrived naked. Two metal ribbon leads were soldered to one side of every cell. This was accomplished with a small soldering iron and 60/40 lead/tin solder. Once completed, ten unit arrays were assembled by soldering the leads of one cell to the back of another in a long chain. To integrate the cells to the wing created a slight problem. The front row could be easily placed upon small styrofoam shelves underneath the coating of plastic, but the back rows needed some way to adhere directly to the covering. Fortunately, a roll of double-sided adhesive was donated by Flexcon Corporation. This adhesive was applied in two half-inch strips to the backside upon which the array rested. To prevent disintegration of this bond and the cells, a small strip of plastic ran along the leading edge of the array and joined the wing approximately 1.5 inches in front of the cells. This prevented the airstream from finding its way underneath the cells and ripping them off.

Stability

Longitudinal and lateral stability were evaluated by classical analysis methods and a study of historical trends.⁷ The horizontal tail and the location of the center of gravity were sized to provide static longitudinal stability.⁸ The effects of expected gust induced loads in the longitudinal direction, pitch, results in a rate of change of the pitching moment with the total airplane lift (dC_M/dC_L) of -0.310 , rendering static stability to the configuration.

Historical trends were studied⁹ and a total dihedral angle of 2.5° was determined to sufficiently ensure roll stability, while not hindering the collection of solar power. A compound dihedral angle was chosen, Figure 19 shows a frontal view of *Surya*. Note the dihedral angle begins at the modular wing connections. The modular wing sections are positioned at an angle of 5° , insuring a total dihedral angle of 2.5° . The vertical tail and dihedral were sized to provide

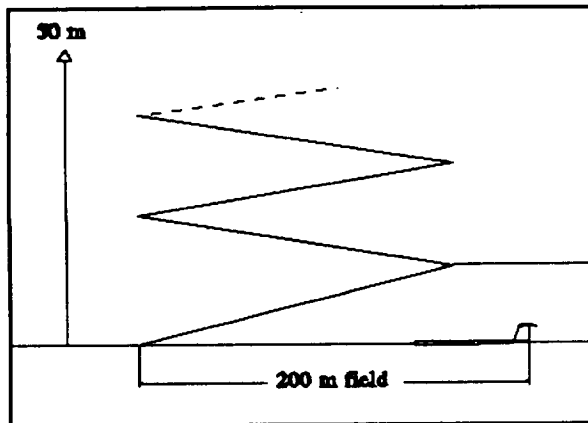


Figure 19: Proposed Climb Scheme

lateral stability. The vertical tail has a Vertical Tail Volume Coefficient of approximately 0.02, typical for a sailplane. The tail has an area of 900 cm², and furnishes directional stability.

The necessary control surface sizes for the plane were determined using a combination of historical trends for similar aircraft¹⁰ and recommendations taken from model aircraft publications. Approximately half of the vertical stabilizer surface area was removed and replaced by a rudder. The rear quarter of the horizontal stabilizer's chord is occupied by an elevator spanning the entire length (1 m) of this component. These control surfaces are actuated by Futaba electronic servos housed within the horizontal stabilizer. Due to the solar cell placement the chord of the ailerons was limited. To conform to the limited width, the ailerons span the entire length of the modular wing sections. The servos that control them are located directly in front of the ailerons, adjacent to the modular wing connections.

Performance and Mode of Operation

Solar propulsion is very appealing on the basis that it is harmless to the environment and cost efficient. The performance of a vehicle, however, is very confined to the weather, time of day, location, season, and efficiency of its solar power system. The available solar cells for this aircraft configuration were not the most efficient or light weight, yet did allow for excess power for take-off and climb. A computer code was developed to predict the performance of the aircraft in level flight.

The aircraft is designed to climb in a circular flight path to an altitude of 50 m in approximately 5 minutes, as shown in Figure 19. This mission requires 5.5 complete revolutions about a 200 m field. The climb rate is a function of the angle of incidence between the sun and the solar cell array, the aircraft climbs at a rate of 0.06 m/s away from the sun and 0.02 m/s towards the sun.

At the design altitude, 18.8 W is required from the

propulsion system to maintain flight at 7.1 m/s. A sustained figure eight flight pattern will be achieved with an angle of attack of 4°, banking angle between 3° and 4°, and a turning radius varying from 67 m to 89 m.

RESULTS & RECOMMENDATIONS

Flight Testing

Surya underwent four flight tests between February and April of 1992. These tests proved not only to be valuable tools in the final design modifications but also as evidence of the sturdiness of the carbon composite structure. Due to the fragility of the solar cells, the first three test flights were completed before the cells were mounted. However, weights were used in place of the solar cells to estimate the behavior of the plane. The first flight test was without propulsion to verify that the location of the center of gravity was the same as that calculated theoretically. In this test, a slight wing twist was detected by the pilot, as well as a shift of the center of gravity from the desired location.

An overcorrected wing twist as well as another shift in the center of gravity persisted in the first powered flight test. The wing twist, now in the opposing direction, was again detected by the pilot. After adjustments were made to correct this by repositioning the modular wing sections, the plane proved to be responsive to controls and relatively easy to maneuver. The second power flight test utilized the propeller's full power, and the need to optimize the propulsion system with a more efficient motor and propeller became evident. Again, the plane responded well to controls and flew for a short amount of time before landing quietly on simple yet effective landing skids.

In the fourth test flight, proxy cell weights were replaced by the actual solar cells. The wing twist was corrected as attested by the pilot. However, the new electronic components installed for the wiring of the cells, shifted the center of gravity once again. This center of gravity shift and the presence of wind gusts caused the climb performance to be sluggish.

Recommendations

Many engineering difficulties were incurred during the design and construction of the solar plane, *Surya*. After the plane construction was completed, there appeared to be many components and processes which could be further optimized through more research, development and testing. Of course many of these revelations were not obvious to the project team before the construction began. The performance of *Surya* depends upon the following criteria: overall efficiency of the propulsion system, structural design, material selection, stability, aerodynamic analysis and the overall weight of the plane.

The efficiency of the propulsion system is determined by its individual components including the solar cells, wiring, motor, propeller and the electronic configurations. It is obvious that the propulsion system is limited by the 12.5% efficient solar cells but the system could be further optimized through improved matching of the motor and propeller. A more efficient motor along with a more powerful propeller would further optimize the propulsion system. To aid in the conservation of the weight budget, that a lighter wire could be used in the solar cell configuration.

Difficulties in maintaining the stability of the plane were experienced during flight testing. The center of gravity was not easily maintained at one tenth of the chord length. The majority of the stability problems could be eliminated by changing the propulsion configuration to include a pusher propeller. This configuration would enable the center of gravity to be kept ahead of the main wing and additional cells to be placed on the horizontal stabilizer. In addition to improved stability, the pusher propeller configuration would allow additional solar cells and power acquired from the cells.

Though *Surya* is structurally sound, the weight of the plane could greatly be reduced in most of the structural components. The handmade carbon composite fuselage and the wing and tail spars could be constructed more exactly to fully optimize the weight. The diameter of the fuselage could be reduced to conserve the weight of the plane. This dimension was originally dictated by a linkage used in the electronics. This linkage was later redesigned so that the fuselage diameter could be reduced. Many processes requiring the application of glue were done using epoxy, which tended to be heavier than standard superglue. Using the glue more sparingly would aid in the minimization of the weight of the plane.

The large size of the plane required that the wing sections of *Surya* be modular. The modular connections of the wing were constructed using a foam and carbon composite combination. These connections could be further optimized to conserve weight and possibly increase stability.

The control surfaces of the plane were increased in size to account for the increase in the size of the entire plane. After completion the plane seemed to be harder to control than had been anticipated. Enlarging the size of the control surfaces would aid in the overall performance of the plane.

The recommendations mentioned above indicate areas in which the design team felt limited. Most of these recommendations occurred at the completion of construction and were realized through experience. Further research and development in these areas are encouraged since the possibilities for various design configurations of this type of aircraft are numerous.

Environmental Impact

Society is faced with various self-induced environmental problems. Implementation of solar energy as a replacement

to traditional energy resources provides an economical solution. The design and construction of this solar powered aircraft attempts to contribute to this cause and encourage future research into alternative energy resources.

ACKNOWLEDGEMENTS

The assistance and technical support of the NASA contacts, Mobil Solar, Aerospace Composites, faculty, staff, students, and many other interested aircraft modelling enthusiasts were numerous and very greatly appreciated. Special thanks to Art Glassman, our NASA/USRA mentor and the advising professors, Prof. William W. Durgin, Prof. Andreas N. Alexandrou, Prof. Ralph F. Cohn, Prof David J. Olinger, Prof. Edward Clarke, and Kurt Heinzmann for their faithful guidance. The educating assistance on aircraft design vital to the required mission provided by Adam Szymkiewicz and Arthur Lavalée has been invaluable. Also thanks to the many helpful staff from WPI especially Todd Billings, Bob Taylor, and Roger Steele for sharing their expertise and equipment.

REFERENCES

- ¹Shevell, R.S., *Fundamentals of Flight*, Prentice Hall, (Englewood Cliffs NJ), 1989.
- ²Shevell, R.S., *Fundamentals of Flight*, Prentice Hall, (Englewood Cliffs NJ), 1989.
- ³Selig et. al., *Soartech 8: Airfoils at Low Speeds*, H.A.
- ⁴Kuethe, A. & Chow, C., *Foundations of Aerodynamics, 4th Ed.*, John-Wiley and Sons, (New York NY), 1986.
- ⁵Shevell, R.S., *Fundamentals of Flight*, Prentice Hall, (Englewood Cliffs NJ), 1989.
- ⁶Hu, C. and White, R.M., *Solar Cells From Basic to Advanced Systems*, McGraw Hill Book Company, (New York NY), 1983.
- ⁷Raymer, D., *Aircraft Design: A Conceptual Approach*, AIAA, Inc., (Washington, DC), 1989.
- ⁸Shevell, R.S., *Fundamentals of Flight*, Prentice Hall, (Englewood Cliffs NJ), 1989.
- ⁹Raymer, D., *Aircraft Design: A Conceptual Approach*, AIAA, Inc., (Washington, DC), 1989.
- ¹⁰Raymer, D., *Aircraft Design: A Conceptual Approach*, AIAA, Inc., (Washington, DC), 1989.

TABLE OF CONTENTS

Chapter 1 Introduction	1
Chapter 2 Aerodynamic Design and Analysis	6
2.1 Introduction	7
2.2 Aerodynamic Configuration	7
2.3 Airfoil Characteristics	8
2.4 Aerodynamic Effects of Solar Cell Placement on Wing	11
2.5 Finite Effects on Wing and Tail	13
2.6 Determination of Total Lift and Drag	15
2.6.1 Total Lift	15
2.6.2 Total Drag Coefficient	15
2.7 Minimum Power Optimization	16
Chapter 3 Structural Analysis	18
3.1 Preliminary Component Sizing	19
3.1.1 Wing Component Sizing	19
3.1.2 Tail Component Sizing	21
3.1.3 Fuselage Component Sizing	21
3.2 Material Selection	22
3.2.1 Construction Process	24
Chapter 4 Stability and Control Surfaces	26
4.1 Stability	27
4.1.1 Static Lateral Stability	28
4.1.2 Static Longitudinal Stability	29
4.2 Control Surfaces	32
Chapter 5 Performance	33
5.1 Level Flight	34
5.2 Climb Performance	35
5.3 Banking and Turning	37
Chapter 6 Solar Cells and Array	39
6.1 Power Requirements and Design Parameters	40
6.2 Photovoltaics and Solar Power	41
6.2.1 Photovoltaic Theory	41
6.2.2 Solar Power Estimation	42
6.2.3 Final Array Size	48
6.3 Array Construction	48
6.3.1 Solar Testing	49
6.3.2 Cell Behavior	50
6.3.3 Array Layout	51
6.3.4 Array Construction	52
Chapter 7 Propulsion and Electronics	54
7.1 Propulsion	55
7.1.1 Motor	55
7.1.2 Propeller	55

7.2 Electronics	.55
7.2.1 Backup Batteries and Power Switch	.55
7.2.2 Controls Wiring	.56
Chapter 8 Results	.58
Chapter 9 Conclusions and Recommendations	.60
References	.64
Appendices	.66

TABLE OF FIGURES

Figure 1.1 <i>Surya</i> Wireframe Model	2
Figure 2.1 The XY Coordinates of the NACA 6409 Airfoil Section	8
Figure 2.2 Sectional Lift & Drag Coefficients of the NACA 6409	9
Figure 2.3 Sectional Lift to Drag Ratio of the NACA 6409	10
Figure 2.4 Inviscid Pressure Distribution of the NACA 6409	11
Figure 2.5 The Modified Flat Back NACA 6409	12
Figure 2.6 Pressure Distribution of the Modified NACA 6409	13
Figure 2.7 Total Lift and Drag Characteristics of the Wing	14
Figure 2.8 Lift and Drag Characteristics at Different AR	14
Figure 2.9 Required Power at Different Flight Velocities	17
Figure 3.1 Wing Loading Model	20
Figure 3.2 Shear and Moment Diagrams	21
Figure 4.1 Degrees of Freedom	27
Figure 4.2 Main Wing Dihedral	28
Figure 4.3 Stability Condition	30
Figure 4.4 Free Body Diagram	30
Figure 5.1 Forces Acting on Plane	34
Figure 5.2 Lift Forces on Plane During Flight	36
Figure 5.3 Proposed Climb Scheme	37
Figure 5.4 Frontal View of Plane During Turn	38
Figure 6.1 Mobil Solar Photovoltaic Cell	41
Figure 6.2 Graph of Power Produced by Cells vs. Time of Day	44
Figure 6.3 Sun Position Angles for Power Calculation	45
Figure 6.4 Typical I-V Curve for Solar Cell	49
Figure 6.5 Typical P-V Curve for Solar Cell	49
Figure 6.6 Experimental I-V Results of Ten Cell Array.	49
Figure 6.7 Experimental P-V Results of Ten Cell Array	49
Figure 6.8 Modular Section of Wing Showing Cell Placement	52
Figure 7.1 Schematic Showing Plane Wiring System	57

CHAPTER 1
INTRODUCTION

As civilization enters the 21st century, considerations for alternative energy sources are becoming necessary. Natural energy sources such as coal, oil, and fossil fuels are quickly depleting. In addition, they have been found to be harmful to the environment. Their use has caused a substantial increase in air pollution, and they have thus been major contributors to the greenhouse effect. Although nuclear energy is immediately available, high operational risks have made it a questionable option. Solar energy is not only pollution free, but it is also available in abundance. Proper utilization of the sun's energy can result in an inexpensive and effective power source. One of the main objectives of the this project is to demonstrate the effectiveness and feasibility of using solar energy to power a small vehicle.

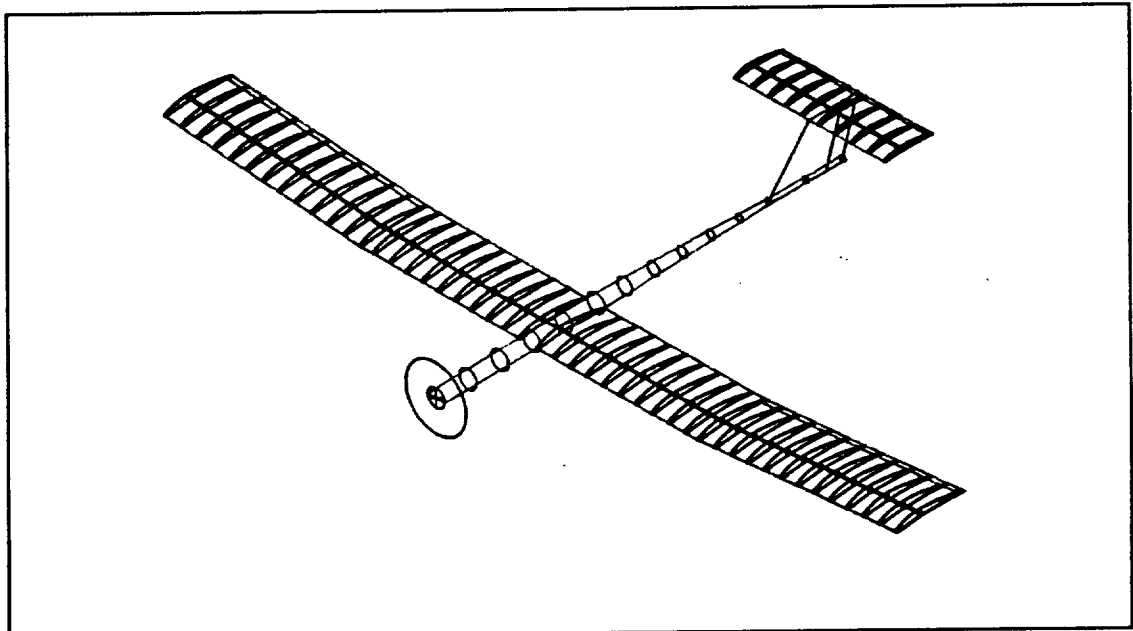


Figure 1.1 Surya: Wireframe Model.

The final configuration of the solar plane was optimized using the concept of minimum power required for level flight. The final wing configuration is summarized as follows. (See Appendix G for color print and dimensions) The wing has a chord length of 42.4 cm and a span is 4.5 m, with an aspect ratio of 10.61. The wing is at a geometric attack angle of 4 degrees and as a result, generates a lift coefficient of 0.8274. The tail is oriented at an angle of attack of 0 degrees and the lift coefficient of the tail is 0.4053. The tail efficiency is assumed to be 0.85 (Shevell, 1983). With this configuration, the solar plane has a total lift coefficient of 0.8816, a total drag coefficient of 0.0451, and the L/D ratio is 19.548.

The design has an overall dihedral of 2.5 degrees (Figure 1.1). The vertical stabilizer has an effective area of 900 cm², the back half of which is taken up by the rudder. Situated 1.6 meters behind the aerodynamic center of the wing, the horizontal stabilizer spans one meter and is composed of a NACA 6409 airfoil with a 30 cm chord. The rear quarter of this chord is a hinged flap which serves as the elevator. The ailerons are located on the modular wing sections, occupying the aft 12% of the chord and spanning their 1 meter length. To ensure pitch stability and optimum lift for the plane as a whole, the center of gravity is maintained a tenth of the wing's chord behind its aerodynamic center. The location of the electronics harness in the nose of the fuselage is adjustable and can be moved either forward or backward to make sure the center of gravity is positioned to maintain static stability.

A total of 120 solar cells are contained within the wing of *Surya*. This number was determined through required power estimations. Conservative estimates predicted about 100 watts for the array output at any given time during flight. Although this

was much less. On an open circuit, the cells developed a potential of 5.8 volts while producing approximately 19 amps of current when short circuited. When a load is applied to the array, these values drop to 4.7 volts and between 12 and 14 amps. To produce this power, 12 arrays containing 10 cells were constructed by hand. The five volt potential is the result of the 10 cells wired in series with each individual cell producing 0.5 volts. The 12 amp current is generated by wiring the 12 sub-arrays in parallel at 1 amp each.

The array itself is split into three rows per wing section. The leading edge row is placed underneath the skin to preserve the integrity of the front part of the airfoil where it is most crucial. The trailing rows adhere directly to the skin on the outside of the wing to increase power production. The first row sits at an angle of 12° with respect to the chord while the back rows sit at an angle of 6° . As a result, optimum power is produced by the array during level flight with the plane flying directly away from the sun.

The minimum level flight speed is the plane speed at which the total drag forces are overcome by the thrust. The plane must remain above this speed to achieve steady level flight. *Surya's* total coefficient of lift was estimated at 0.88, and both the tail and the wing act as lifting surfaces. With a weight of 52 N (Appendix F), and an estimated parasitic drag coefficient at 0.148, the plane is expected to have a minimum flight speed of 7.1 m/s and a minimum required power to achieve this speed of 18.8 Watts.

The climb capability of the plane is strictly determined by the amount of excess power available. After initial energy is expended for level flight, the remaining power which is available from the power source is used for climbing. *Surya's* climb rates vary depending on the output of power from the solar cells at that time interval, and the

position of the plane relative to the sun.

Banking and turning is another basic maneuver at which the plane must remain in level flight. Since the flight velocity of the solar plane is low, the banking angles are small. With small banking angles of between 3 and 4 degrees, the turn radii necessary are 89 and 67 m respectively. Hence, the proposed spiral climb scheme for the 50 m altitude climb can be accomplished in about five minutes within a 200 m length field.

To obtain the final design the group was split into four different sub-groups, dealing with Aerodynamics, Performance and Stability, Structure, and Solar Power. In the following chapters, the analysis of each sub-group and justifications for its results are presented.

CHAPTER 2
AERODYNAMIC DESIGN & ANALYSIS

2.1 Introduction

In this chapter, the aerodynamic considerations of the design, such as the airfoil characteristics, finite wing and tail effects, optimization for minimum power, and the overall aircraft configuration are discussed. Since the proposed design is a low velocity plane, the chord Reynolds number is relatively low. Theoretically, viscous effects dominate the flow at low Reynolds numbers, thus resulting in flow separation and a laminar separation bubble. However, at Reynolds number of 200,000 or higher, a turbulent boundary layer develops and gives more resistance to flow separation during the pressure recovery. For this reason, it was decided to operate the plane at a chord Reynolds number of about 200,000. In addition, the effects of compressibility are neglected in the entire aerodynamic analysis, since the Mach number during level flight is much less than 0.3.

2.2 Aerodynamic Configuration

The final configuration of the aerodynamic design is summarized in this section. The wing section was chosen to be the NACA 6409. The wing has a rectangular platform with a wing span of 4.5 meters and a chordlength of 0.424 meters. The aspect ratio of the wing is 10.61 and the geometrical angle of attack is 4 degrees. The wing generates a lift coefficient, C_L , of 0.8274 at level flight conditions. The NACA 6409 airfoil was also chosen for the tail section. The tail has a rectangular platform, a tail

span of 1.0 meter and a chordlength of 0.3 meters. The resulting aspect ratio of the tail is 3.333. At level flight conditions, the geometrical angle of attack is 0 degrees and the C_L of the tail is 0.4053. The tail efficiency was assumed to be 0.85 (Shevell, 1983). With this configuration, the aircraft has a total lift coefficient of 0.8816 and a total drag coefficient of 0.0451. As a result, the total lift to drag ratio is equal to 19.548.

2.3 Airfoil Characteristic

The NACA 6409 was chosen as the airfoil section for the wing and the tail.

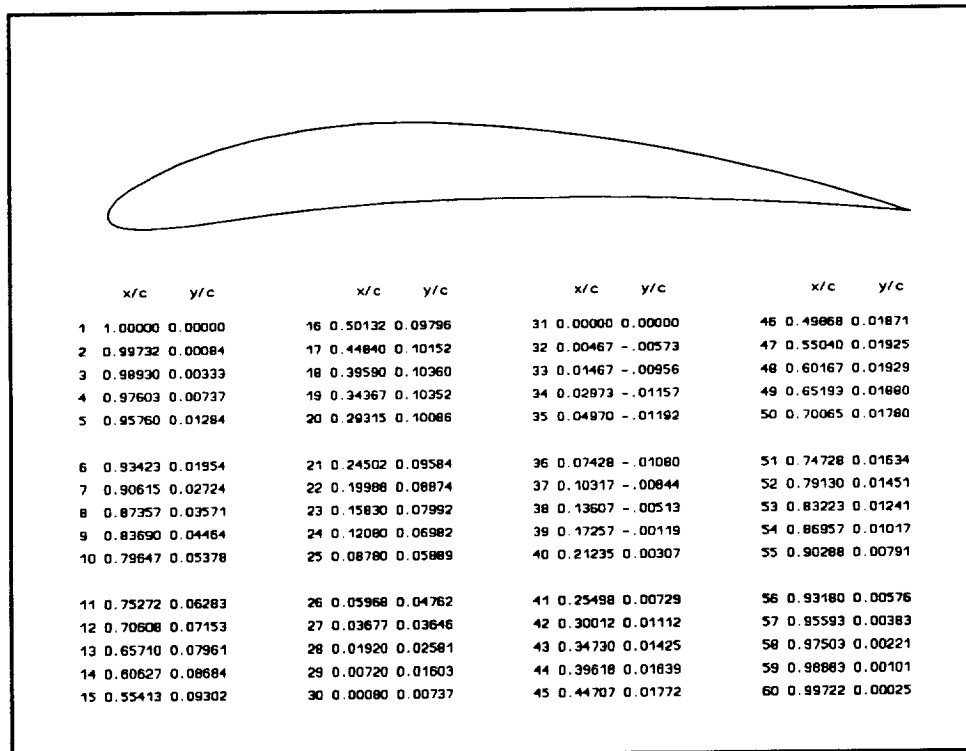


Figure 2.1 The X-Y Coordinates of the NACA 6409 Airfoil Section.

It has a 9% maximum thickness and a 6% maximum chamber at a distance of 40% of the chord from the leading edge. The coordinates of the airfoil are summarized in Figure 2.1.

Figure 2.2 shows the experimental lift and drag characteristic of the NACA 6409 airfoil at the Reynolds number of 200,100 (Selig et al., 1989). The sectional lift curve slope of the airfoil is about 5.17 per radian between an angle of attack of -0.87 and 7.32 degrees. At an angle of attack of 9.32 degrees, the sectional lift coefficient reaches a maximum value of 1.342 . Meanwhile, the sectional drag coefficient varies parabolically and has a minimum drag coefficient of 0.0112 at an angle of attack of 1.20 degrees.

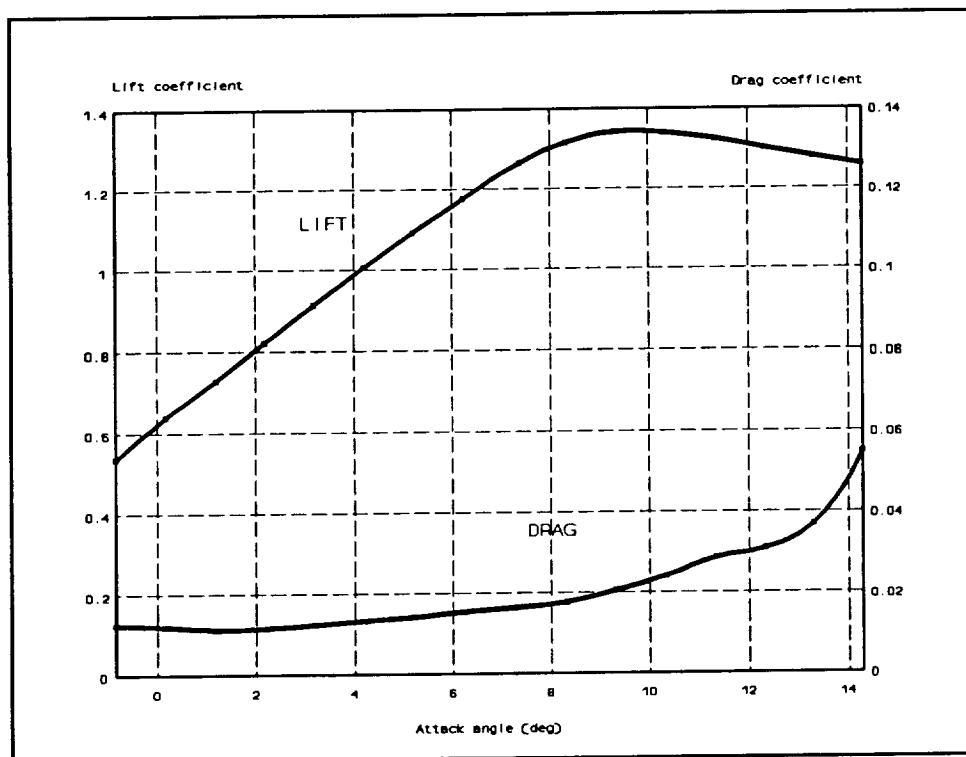


Figure 2.2 Sectional Lift and Drag Coefficients for the NACA 6409 Airfoil.

The lift to drag ratio of the airfoil is calculated and summarized in Figure 2.3. As shown in the figure, the airfoil provides a constant high lift to drag ratio between the angles of attack of 2 and 8 degrees. Therefore, it gives a wide range of favorable operating conditions.

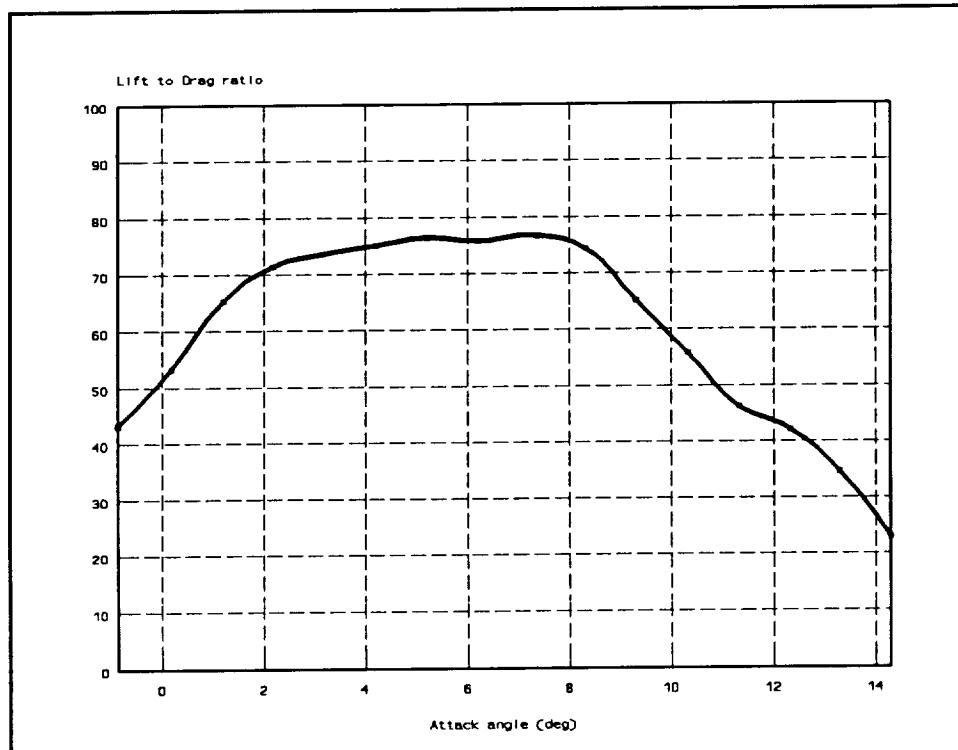


Figure 2.3 Sectional Lift to Drag Ratio of the NACA 6409 Airfoil.

2.4 Aerodynamic Effects of the Solar Cell Placement on Wing

In order to increase the power generated by the solar cells, it was decided to place the cells on the surface of the wing. Since the solar cells are flat and not flexible, the shape of the airfoil is slightly changed. As a result, the sectional characteristic of the airfoil are affected. By using the vortex panel method (Kuethe, 1986), the inviscid pressure distribution of the original NACA 6409 was calculated as shown in Figure 2.4.

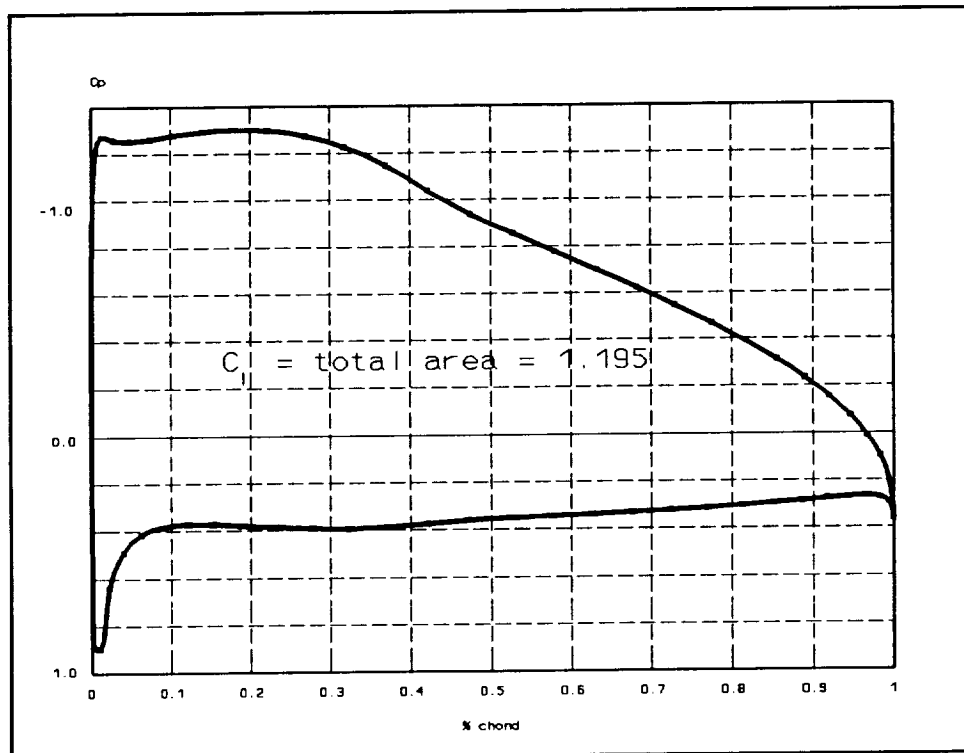


Figure 2.4 Inviscid Pressure Distribution of the NACA 6409 Airfoil.

In the figure, it is clearly shown that the majority of the lift is generated in the front 40% of the airfoil. Therefore, in order to minimize the aerodynamic effects due to the solar cells placement, the cells were placed behind a distance of 40% of the chord from the leading edge (Figure 2.5). The inviscid pressure distribution of the airfoil which has

the solar cells on the back is shown in Figure 2.6. At an angle of attack of 4 degrees, the difference between the inviscid lift coefficients of the original airfoil and the one which has solar cells on the back is only about 0.25%.

With the assumption that the flow does not separate before the first 40% of the chord, the aerodynamic characteristics of the modified airfoil are apparently similar to the original NACA 6409. Therefore, the experimental data of the NACA 6409 airfoil are assumed to be valid for the design

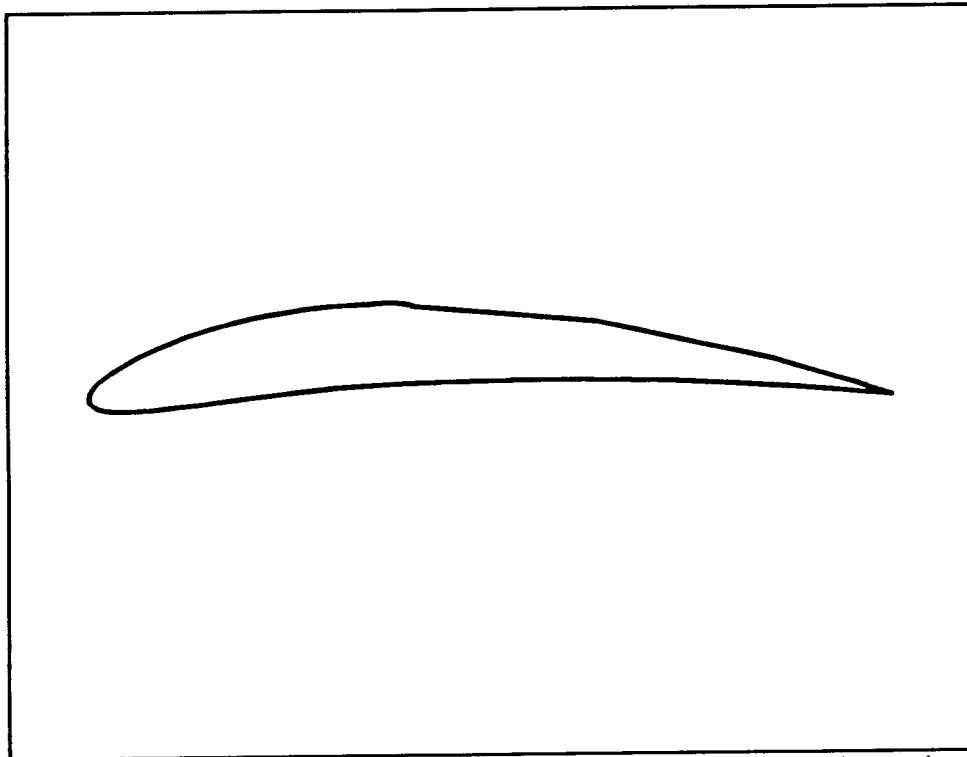


Figure 2.5 The Modified NACA 6409 Airfoil with Flattened Back.

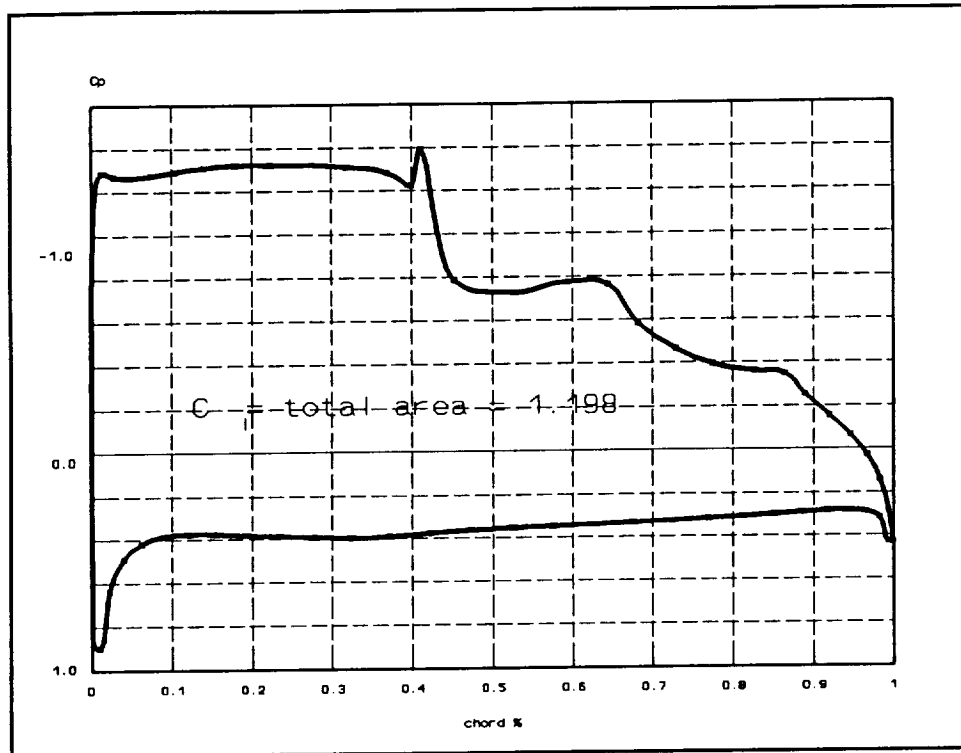


Figure 2.6 Inviscid Pressure Distribution of the Modified NACA 6409 Airfoil.

2.5 Finite Effects on Wing and Tail

By using the Glauert Method (Appendix A.1) and the modified flat plate theory (Shevell, 1983), the finite lift and drag coefficients of the wing and tail are determined. Figure 2.7 shows the finite lift and drag characteristic of the wing at different attack angles. In addition, the aspect ratio effects to the L/D ratio are investigated. With a higher aspect ratio, the wing behaves closer to the predicted performance of the airfoil section. As a result, the wing generates more lift and experiences less induced drag. In Figure 2.8, it shows clearly that the lift to drag ratio increases while the aspect ratio of the wing increases.

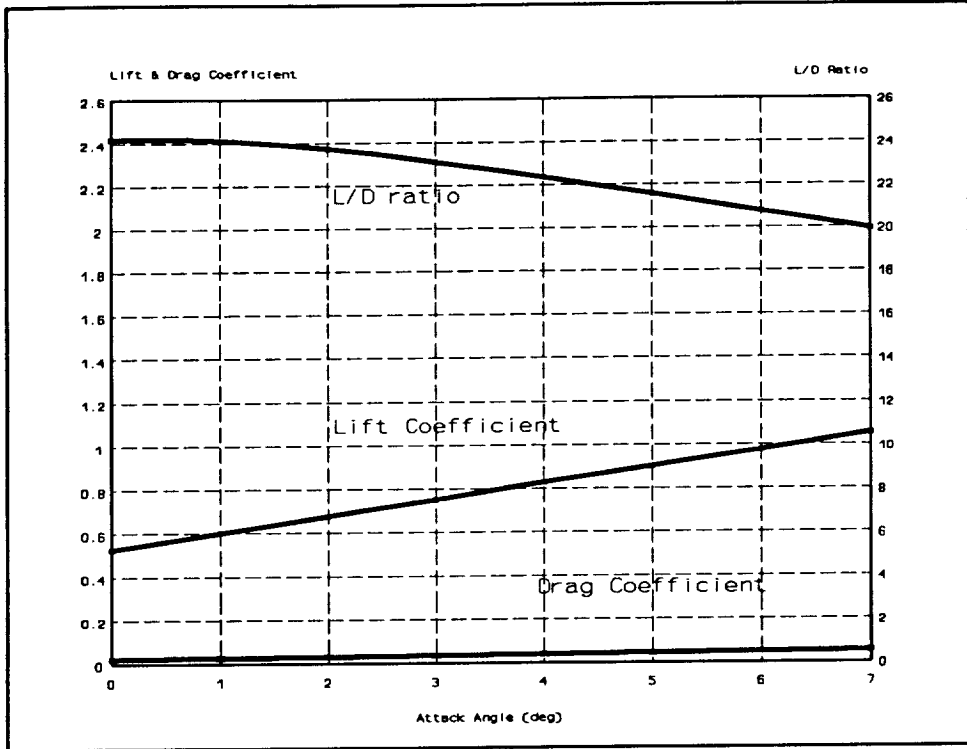


Figure 2.7 Lift and Drag Characteristics of the Finite Wing.

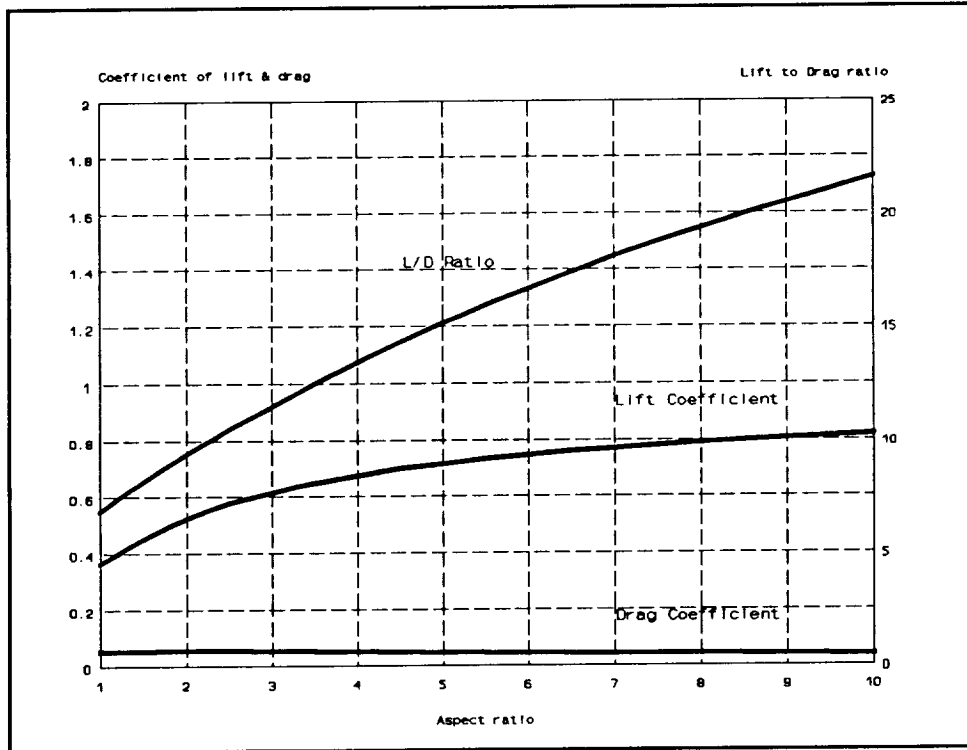


Figure 2.8 Effects of Aspect Ratio on Lift and Drag.

2.6 Determination of Total Lift and Drag

2.6.1 Total Lift

In determining the total lift coefficient of the solar plane, it was assumed that the wing and the tail will contribute to the lifting forces. The lifting effects of the fuselage and vertical tail were neglected. Therefore, the lift coefficient of our design is expressed as follows:

$$C_L = C_{L_w} + \eta_t \left(\frac{S_t}{S_w} \right) C_{L_t} \quad [2.1]$$

where C_{L_w} and C_{L_t} are the lift coefficients of the wing and the tail with respect to their own planform areas. S_w and S_t are the planform areas of the wing and the tail, respectively. However, η_t represents the tail efficiency which is defined as the ratio of dynamic pressure at the tail to that of the free stream.

2.6.2 Total Drag Coefficient

As shown in equation 2.2, the total drag coefficient of the airplane is described as the sum of the parasitic drag and the induced drag coefficients.

$$C_D = C_{D_p} + \frac{C_L^2}{\pi (AR) e} \quad [2.2]$$

where C_{D_p} is the total parasitic drag coefficient with respect to the wing planform area.

C_{DP} is evaluated by using the modified flat plate theory (Shevell, 1983). However, C_L represents the total lift coefficient, AR is the aspect ratio of the wing, and e is the Oswald airplane efficiency which relates to the deviations from the ideal elliptical lift distribution.

2.7 Minimum Power Optimization

Since the solar plane is propeller driven, the optimum operating condition or the maximum endurance will occur at the speed when the required power is minimum. However, the required power for level flight can be written as:

$$P = D \cdot V \quad [2.3]$$

By substituting the induced drag coefficient and the level flight velocity in terms of C_L and taking the derivative with respect to C_L , we can get the following relationships:

$$C_{L_{\min. power}}^2 = 3 \pi C_{DP} \cdot AR \cdot e \quad [2.4]$$

and

$$C_{D_{i \min. power}} = \frac{3 \pi C_{DP} \cdot AR \cdot e}{\pi \cdot AR \cdot e} = 3 C_{DP} \quad [2.5]$$

As a result, the induced drag coefficient is three times larger than the parasitic drag coefficient at the minimum power condition. For our design, the power required for level flight at different velocities is calculated and summarized in Figure 2.9.

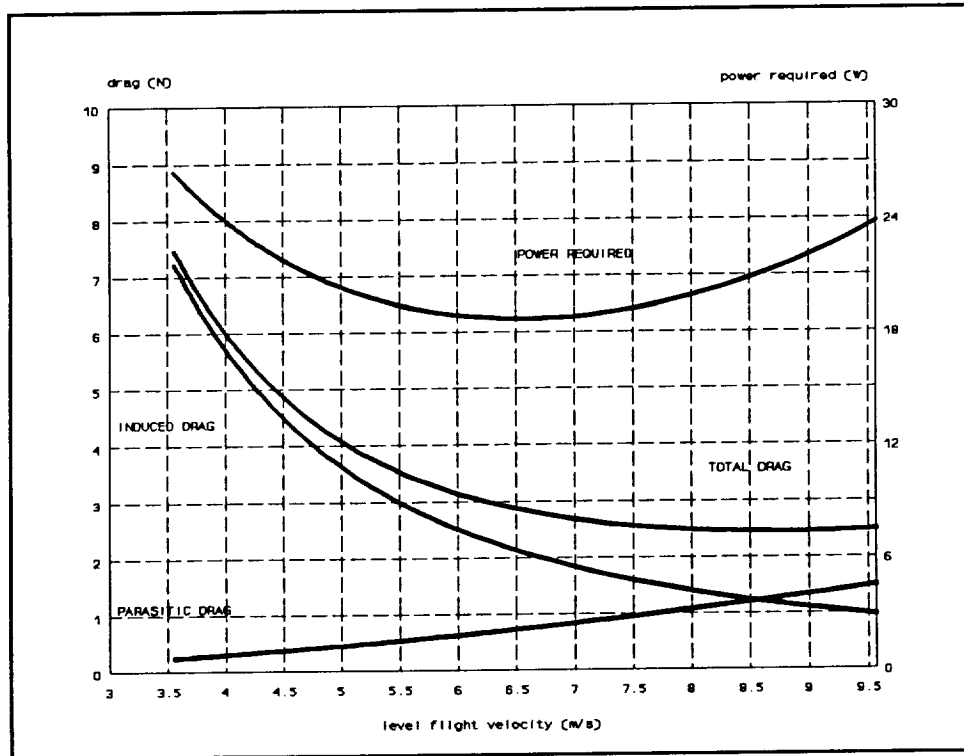


Figure 2.9 Required Power at Different Level Flight Velocities.

The figure shows that the optimum level flight speed is 6.388 m/s and the corresponding attack angle is 6.77 degrees. At this condition, the power required for level flight is equal to 18.682 Watts. Unfortunately, the linear region of the sectional lift curve is between the attack angle of -0.87 and 7.32 degrees. Apparently, the attack angle at the optimum condition is close to the upper boundary of the linear region. Due to safety considerations, it was decided to operate at an attack angle of 4 degrees, with the corresponding cruising speed is 7.104 m/s. However, the required power is 18.839 Watts and which is 0.84% higher than the power required at the optimum condition.

CHAPTER 3
STRUCTURAL ANALYSIS

3.1 Preliminary Component Sizing

Preliminary component sizing was dictated by set parameters such as the chosen airfoil, the size of the solar cells, and the desired lift to drag ratio. The resulting configuration had a wing span of 4.5 meters, a tail span of 1 meter, and a fuselage length of 2.5 meters. Due to the large span, the wing had to be modular for storage purposes. This section describes the techniques used to determine the size of the components, the material selection, and the stress analysis of the aircraft.

3.1.1 Wing Component Sizing

The span of the wing was dictated by an optimization of the lift to drag ratio determined by the aerodynamics group. The primary wing section, i.e. not including modular tips, has a length of 2.5 meters. Each modular section is 1 meter long, and connected to the primary wing at a 5 degree dihedral with respect to the horizontal.

The main supporting structure of the wing is a rigid tube running the length of the span, effectively acting as a wing spar. The initial sizing of the spar involved the selection of material and dimensions of the cross section. The outer diameter of the tube was limited by the thickness of the airfoil. The thickness of the tube was determined by a simplified stress analysis of the loads applied to the spar.

A simplified half wing loading model was developed to estimate the maximum stress on the wing spar. The carbon spar was to assume all of the lift loads. The wing was modeled as a cantilevered beam with a distributed load, and a moment load applied

at the free end.

The distributed load depicts the lift applied along the primary wing section. The resulting force created by the modular section was represented by the moment applied at the free end of the beam. This moment occurs at the connection

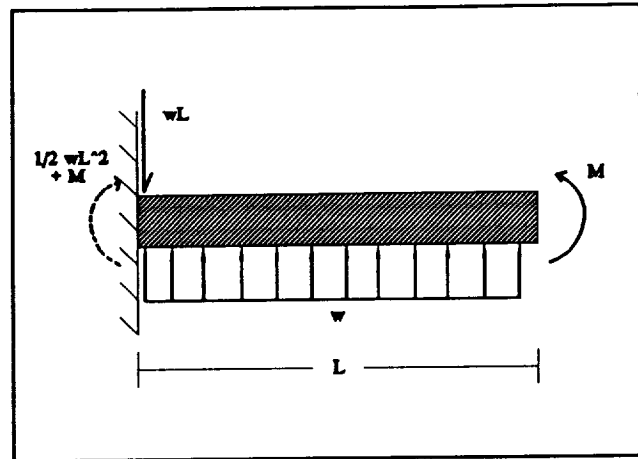


Figure 3.1 Wing Loading Model

point. An illustration of this model is seen in Figure 3.1.

A lift of 48.3 Newtons was calculated by the aerodynamics group. This force was represented by a distributed load of 10.73 Newtons per meter acting along the full span. The distributed load acting on the modular section produces an effective moment of 5.36 N*m located at the connection point, shown at the free end of the beam. These calculations were then adjusted to account for the potential gust load the wing may endure. With a gust load factor of 3, the loads were increased to a distributed load of 32.19 N/m and an effective moment of 16.09 N*m.

The shear and moment distributions of the wing are illustrated in Figure 3.2. The locations of maximum shear and maximum bending moment were determined from these diagrams. The maximum shear was calculated to be 40.24 N. The maximum moment, calculated by summing applied moments on the primary wing section, was 41.24 N*m.

The final dimension to be sized was the thickness of the hollow spar. This dimension is dependent upon the properties of the chosen material and the maximum stress on the spar resulting from the applied loads. Only normal stress was considered; shear stress was determined to be negligible in comparison.

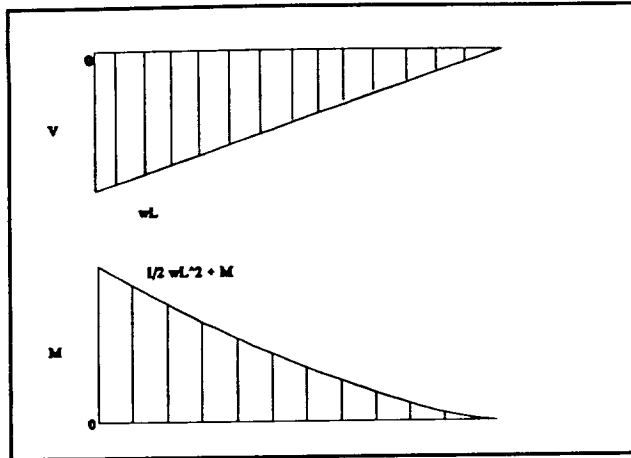


Figure 3.2 Shear and Moment Diagrams

The carbon composite spar was constructed by hand and testing was conducted to obtain accurate material properties (Appendix B.1). From the maximum applied load, and safety factor of 1.2, the maximum allowable stress for the spar to assume was calculated. The minimum required

spar thickness was then determined through iteration. See Appendix B.2 for the calculations and accompanying computer program.

The dimensions of the wing spar resulting from this analysis are a 2.01 cm diameter tube, 0.53 mm thick (3 layers of fabric), with an inner diameter of 1.90 cm.

3.1.2 Tail Component Sizing

The loading model and dimension analysis for the tail spar was performed similarly to that of the wing. The lift was represented as a constant distributed load along the tail spar. Again, a cantilever beam model was used as in the wing, differing only by the absence of the moment at the free end.

The lift on the tail was calculated by the aerodynamics group as 3.7 Newtons. Thus, the distributed load was 3.7 Newtons per meter. The method for sizing the tail spar was identical to that of the wing. The resulting tail spar dimensions are an outer diameter of 1.38 cm and a thickness of 0.53 mm (3 fabric layers).

3.1.3 Fuselage Sizing

The remaining structural component to be sized was the fuselage. The length of the fuselage was dependent on the placement of the tail and the area required to house the electronics. This length was determined to be 2.5 meters. The anterior portion of the fuselage is 10.5 cm in diameter, which was determined by an estimation of the size of the electronic components. This diameter gradually decreased with length in order to minimize weight. The posterior segment has a diameter of 3 cm. This value was determined to be the minimum within the margin of safety. The required thickness of the fuselage wall for this design was 0.36 mm.

3.2 Material Selection

The material selection process played a key role in the design configuration. Since the power available from the solar cells necessitated the minimization of weight, effective material selection was crucial in the design process. While the weight of the structure needed to be minimized, a high strength material was desired to withstand the applied loads. This necessitated research into composite materials because they exhibit a high strength to weight ratio.

Many composite fabrics were tested including carbon, kevlar, and fiberglass. Carbon was selected due to its high strength to weight ratio and inherent rigidity. Consequently, the wing spar, tail spar, and fuselage were constructed using this material. Furthermore, we tested a number of different spar configurations to determine the material constraints at different loads. These tests led to the selection of a hollow rod cross section configuration. Sample hollow rod configurations were tested in the lab to

determine the thickness of the tube required to withstand the expected stress (Appendix B.1).

The vertical stabilizer which supported the tail spar was constructed using a foam structure which was reinforced with carbon composite fabric on both sides. The carbon composite provided the strength needed to support the tail and foam was used as a spacer.

Since the wing spar was modular, a connecting support was used to form the dihedral angle in the wing and withstand the load applied at the connection. The modular connection supports utilized a foam and carbon composite combination much like that of the vertical stabilizer with foam sandwiched between two layers of carbon composite fabric.

Foam was used as a spacer in the vertical stabilizer and modular connection supports because of its low density making it the most lightweight material used in the plane. The carbon composite fiber and foam combination proved to be ideal when used on components that were designed to withstand pure bending loads. Foam was used to construct components exhibiting no structural applied loads such as the solar cell braces, nose cone, and wing tips.

Balsa wood was utilized for many components that sustained small loads and required a precise shape. Since balsa is the lightest of all wood and very easily shaped it was favored over foam. Balsa wood was used for components such as the ribs, the leading and trailing edges, the ailerons, the elevator, and the horizontal stabilizer. The ailerons and the horizontal stabilizer utilized balsa wood in a truss structure designed as an extension of the airfoil.

The last essential component requiring a material selection was the skin. Heat

shrinking mylar was used for this application. It was necessary to use a material with a high transmissivity on the top of the wing so sunlight could reach the solar cells underneath the skin, but at the same time the material had to be strong enough to sustain the shape of the airfoil it formed. Another concern about the material of the skin was a desired resistance to tear as deformation of the wing was experienced. Mylar becomes rigid after being heat shrunk over a surface but it remains adequately flexible enough to deform.

3.2.1 Construction Process

Test performed with carbon composites indicated that with an application of epoxy resin, the fabric could be molded into different formations. The construction of the wing spar began after, the minimum number of times the fabric needed to be wrapped around a mold was determined. This was dictated by the minimum thickness calculated according to the method documented in Appendix B.2 .

As a result of these calculations, it was determined that the wing spar required three layers of fabric while the tail spar and fuselage required two. A piece of ordinary PVC tubing of the desired diameter served as the mold after it was wrapped in mylar to prevent any adhesion to the resultant carbon tube.

The fuselage mold was constructed using PVC tubing of the desired diameters with a tapered section made of foam connecting them. A microlyte filler was applied to the finished carbon structure to smooth out the imperfections that inevitably existed. The main wing was connected to the fuselage by drilling a hole through the fuselage and passing the wing tube through the center of the body. The connection was reinforced using carbon fiber sleeves. Subsequent tasks included gluing the ribs to the wing spar,

applying the mylar, and wiring all of the electrical components and solar cells.

CHAPTER 4
STABILITY AND CONTROL SURFACES

4.1 Stability

Stability can be divided into static and dynamic stability. Static stability, a requirement for flight, refers to the system's immediate reaction to an aerodynamic disturbance. A statically stable aircraft will return back towards its equilibrium position if it is disturbed by a gust of wind, while an unstable plane would continue to stray from straight and level flight.

Dynamic stability deals with the history of the craft's motion after the disturbances, in particular whether or not the induced motion dampens out. In full scale aircraft, dynamic stability is optimized to facilitate simple, steady flying characteristics during cruise, so a pilot doesn't have to devote all his concentration to working the controls. The nature of flying model aircraft, however, demands the pilot's constant attention, due to relatively low altitudes and increased susceptibility to gust disturbance.

The six degrees of freedom of an aircraft's motion can be separated into two independent groups, lateral and longitudinal (Figure 4.1). Lateral motions include rolling, yawing and sideslipping, while the longitudinal motions are made up of motion along the flight path, vertical motion, and

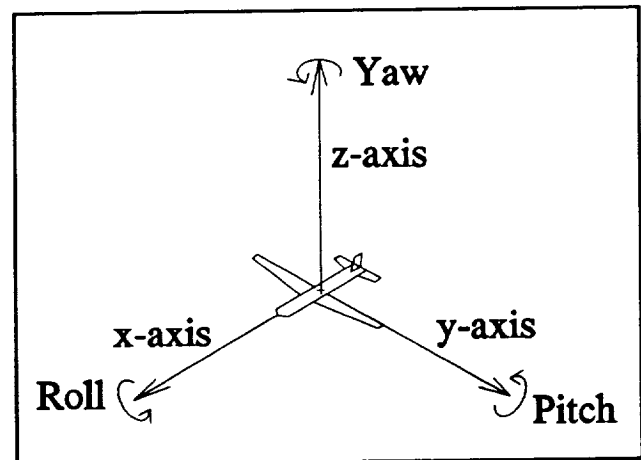


Figure 4.1 Degrees of Freedom

pitching. Since these groups are independent of each other, their stability, whether it is static or dynamic, can be studied independently.

4.1.1 Static Lateral Stability

Static lateral stability can be further divided into two types, dihedral stability and directional stability.

Dihedral, or "roll" stability is the plane's tendency to return to equilibrium after a banking maneuver. This form of stability is ensured by inclining the wings at a slight "dihedral angle" so that the wing tips are higher than the wing root. When in a bank, an aircraft will experience sideslip. As the plane slips, the presence of a dihedral angle increases the effective angle of attack of the lower wing, and decreases it on the upper wing. This causes a respective increase in lift on the lower wing and a decrease in lift on the upper wing, therefore forcing the plane to roll back to level conditions. For *Surya*, historical trends were studied (Raymer, 1989) and a total dihedral angle of 2.5 degrees was chosen as sufficient to ensure roll stability, while not hindering the collection of solar power.

The main wing spar is a straight, continuous tube that passes through the fuselage, from one modular wing connection to the other. This was done to insure maximum strength at the wing root, where it is needed most. With this in mind, and to minimize construction difficulties, a compound dihedral configuration was chosen for *Surya*.

Figure 4.2 shows a frontal view of the solar plane. Notice that the dihedral

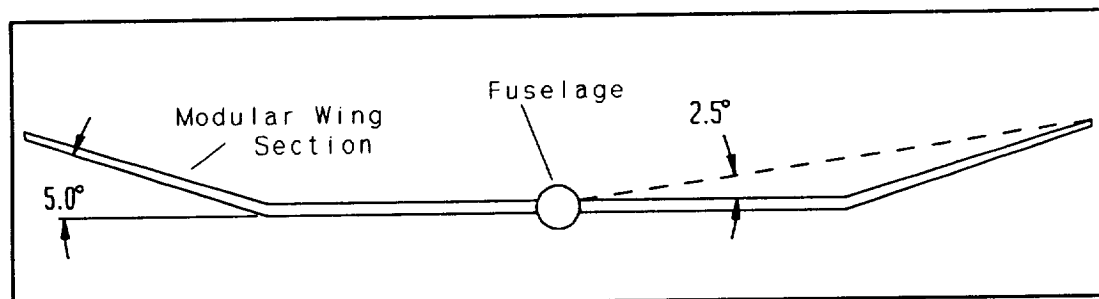


Figure 4.2 Main Wing Dihedral

angle begins at the modular wing connections. To insure a total dihedral angle of 2.5

degrees, the modular wings are positioned with a dihedral of 5° , so a line drawn from the wing root to the wing tip shows the necessary angle of 2.5 degrees.

Directional or "weathercock" stability is the tendency of the aircraft to point into the oncoming air flow. A proper size and location for the vertical tail will guarantee directional stability. Historical trends were again used (Raymer, 1989) to find a comparable Vertical Tail Volume Coefficient (c_{vt}). Once design parameters such as wing area (S_w), wing chord (b_w), and tail moment arm (L_t), were determined in other parts of the conceptual design, the vertical tail surface area (S_{vt}) could be calculated using equation 4.1.

$$S_{vt} = \frac{c_{vt} b_w S_w}{L_t} \quad [4.1]$$

Surya's vertical tail has an area of 900 cm^2 , as required for proper directional stability.

4.1.2 Static Longitudinal Stability

For an aircraft to sustain flight it must maintain the proper airspeed and angle of attack to avoid stalling the main wing. Since these two parameters are directly affected by pitch, static longitudinal, or "pitch" stability is the most critical stability condition. To ensure this, the aircraft's configuration must exhibit a negative change in its' moment coefficient for every positive change in its' lift coefficient, or:

$$\frac{dC_M}{dC_L} < 0 \quad [4.2]$$

Since the coefficient of lift is directly proportional to the angle of attack, this condition could be graphically represented as

in figure 4.3. A pitch up disturbance that increases the wing's angle of attack (α), will cause the moment coefficient (C_M) to decrease. This decrease in moment coefficient forces the wing to pitch back down, countering the affect of the

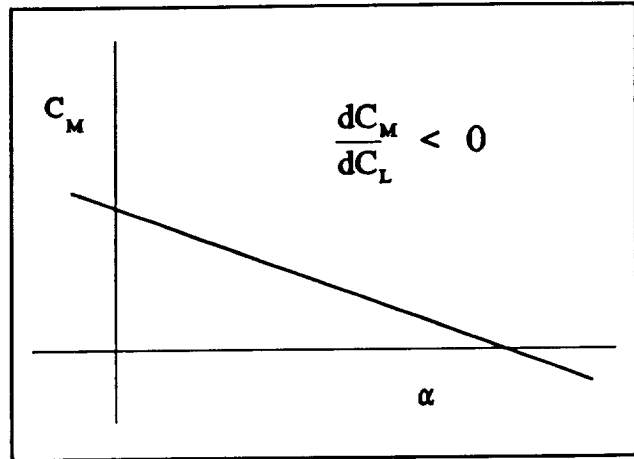


Figure 4.3 Stability Condition

disturbance. Since moments are what cause aircraft to pitch, the first step towards an equation for measuring static longitudinal stability, is to examine the moments that affect an airplane.

Figure 4.4 is a free body diagram of a simple airplane, where "L_w" is the lift generated by the main wing "M_{ac}" is the moment generated about the aerodynamic center of the main wing, "L_H" is the horizontal tail's lift, "x_{cg}" is the distance from

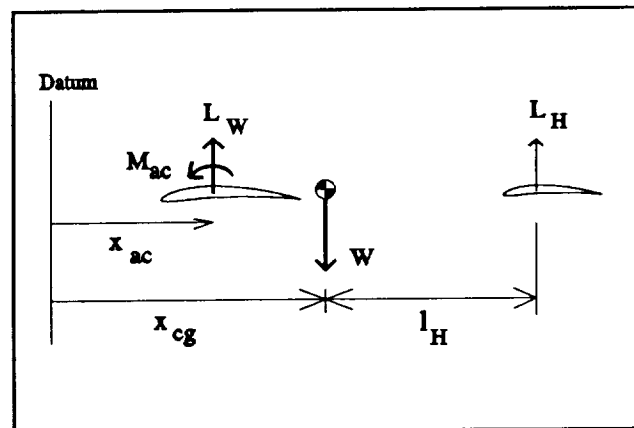


Figure 4.4 Free Body Diagram

the datum to the center of gravity, "x_{ac}" is the distance to the aerodynamic center of the main wing, "W" is the system's total weight, and "l_H" is the distance from the center of gravity to the aerodynamic center of the horizontal tail. Summing the moments in figure 4.4 gives the equation:

$$M_{cg} = M_W - M_H + M_F \quad [4.3]$$

Moments produced by the wing (M_w) include, the moment that is always produced

about the aerodynamic center of a lifting airfoil (M_{ac}), and the moment that is composed of the main wing's lifting force and its distance from the center of gravity. The horizontal tail's moment (M_H) is created by the lift it produces and its distance from the center of gravity. Moments created by the Fuselage (M_F) are small in *Surya*'s case and can be neglected. Making the proper substitutions results in:

$$M_{cg} = M_{ac} + L_w(x_{cg} - x_{ac}) - L_H(l_H) \quad [4.4]$$

Now dividing through by the dynamic pressure at the wing (q_w) will convert the moments to moment coefficients, and non-dimensionalize the "x" distances:

$$C_{M_{cg}} = C_{MAC} + C_L\left(\frac{x_{cg}}{c} - \frac{x_{ac}}{c}\right) - C_{L_H}\left(\frac{q_H}{q_w}\right)l_H \quad [4.5]$$

Finally differentiating with respect to the coefficient of lift and manipulating, reveals the equation used to measure static longitudinal stability.

$$\frac{dC_M}{dC_L} = 0 + \left(\frac{x_{cg}}{c} - \frac{x_{ac}}{c}\right) - \left(\frac{a_H}{a_w}\right)\eta_H V_H \frac{d\alpha_H}{d\alpha_w} \quad [4.6]$$

where:

- a_w - is the lift curve slope for the main wing
- a_H - is the lift curve slope for the horizontal tail
- η_H - is the horizontal tail's efficiency
- V_H - is the volume of the horizontal tail
- $d\alpha_H/d\alpha_w$ - is a measure of the downwash affect on the tail

As was stated earlier, for a design to maintain proper static longitudinal stability, dC_m/dC_l must be less than zero. For *Surya*, with its' center of gravity located a tenth of the wing chord behind the aerodynamic center of the main wing:

$$\frac{dC_M}{dC_L} = -.310 \quad [4.7]$$

Appendix C contains a copy of the computer program used to calculate these numbers during the design sessions.

4.2 Control Surfaces

The necessary control surface sizes for the solar plane were determined using a combination of historical trends for similar aircraft (Raymer, 1989), and recommendations taken from model aircraft publications.

As stated in the previous section, the vertical stabilizer was sized using stability criteria. Following recommended practices approximately half of this area was then removed and replaced by a rudder made from balsa wood. The rear quarter of the horizontal stabilizer's chord is occupied by the elevator. It spans the entire length of one meter and is actuated, like the rudder, by a Futaba electronic servo housed inside the horizontal stabilizer.

Due to solar cell placement on the back of the airfoil, the chord of the ailerons was limited. To make up for their limited width, the ailerons span the entire length of the modular wing sections. The servos that control them are located directly in front of the ailerons, adjacent to where the modular wings connect to the central wing section.

CHAPTER 5
PERFORMANCE

The performance analysis consists of the level flight capability, climb capability, and turning maneuvers. Level flight is the main criterion for which the others are determined. In all the conditions, the plane must demonstrate its ability to maintain steady flight, hence ensuring minimal flight capability.

5.1 Level Flight

The most basic flight condition is that of level flight. At this condition, the major forces which act on an airplane are in equilibrium. (Fig. 5.1) The weight of the plane is balanced by the lift generated and the thrust of the plane is also equally opposed by the drag.

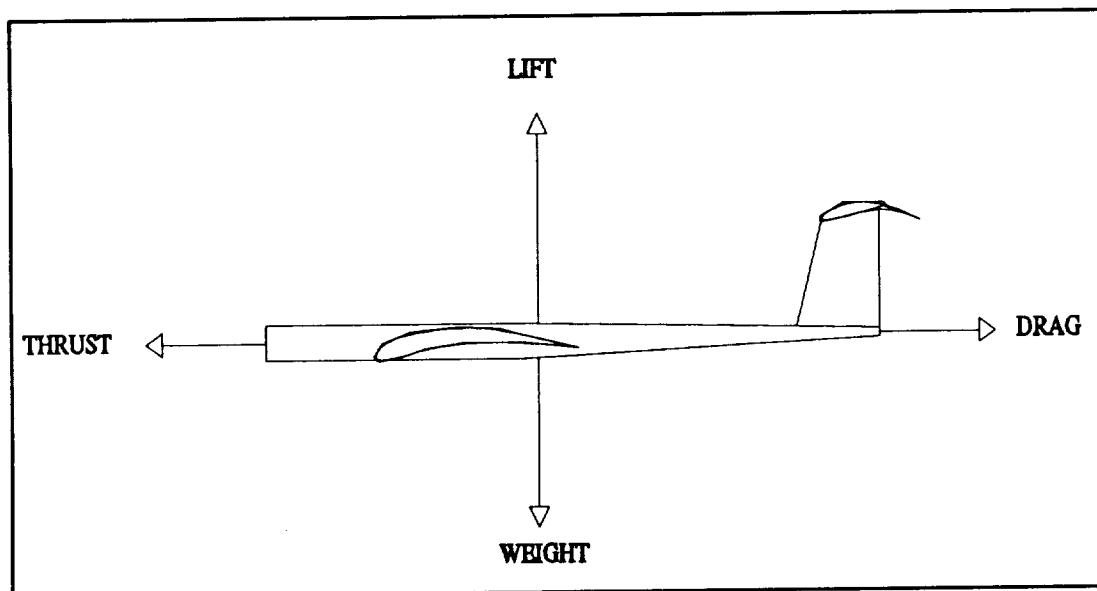


Figure 5.1 Forces acting on plane

The current design configuration utilizes both the wings and horizontal stabilizer as lifting surfaces.

In level flight conditions, the amount of lift produced equals the weight of the plane. The coefficient of lift was calculated through the aerodynamics analysis. The same analysis yields the minimum level flight speed from which the minimum required power is determined. This minimum power is determined by,

$$Power = Drag \times Velocity \quad [5.1]$$

Both parasitic and lift induced drag contribute to the total drag force on the airplane during flight. The drag force due to the compressibility of air is neglected due to the low velocities involved. The ability to achieve level flight is directly related to the plane's ability to generate enough thrust and lift to overcome the total drag and weight. The minimum power required for this plane with an estimated weight of 52 N and a minimum level flight velocity of 7.1 m/s, is 18.8 Watts. The computer program which was developed to calculate minimum level flight velocity and power is included in Appendix D.

5.2 Climb Performance

Part of *Surya's* mission is to climb to a flight altitude of 50 m. The plane's ability to achieve this is measured by the rate of climb.

Climb performance depends on the excess power available from the solar array that is not already used for level flight. During climb, the perpendicular force of lift is changed due to the placement of the aircraft. (Fig. 5.2) However, since the level flight velocity is relatively low, the climb angle will be small. Hence, the lift component, $L \cos \beta$, can be approximated by L .

The rate of climb is defined as the excess power available divided by the lift produced. Since lift is equal to weight for small climb angles, rate of climb is defined as:

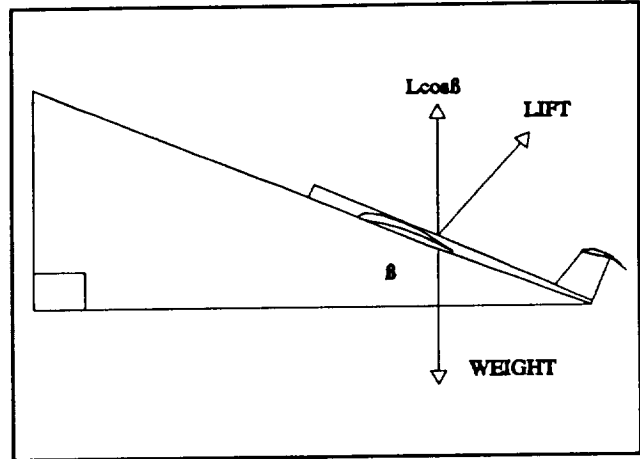


Figure 5.2 Lift forces on plane during climb

$$\frac{dH}{dt} = \frac{\text{Power}_{\text{excess}}}{\text{Weight}} \quad [5.2]$$

This number varies depending on the position of the solar cells relative to the sun. Depending on the positioning of the plane in flight, the rate of climb that can be achieved varies from 0.02 m/s to 0.06 m/s.

To meet the mission requirement of reaching an altitude of 50 m, a straight ascent path results in a horizontal ground distance of over 2000 m. The area available to fly the plane was limited to a maximum field length of 200 m. Therefore, an upward spiral climb scheme is utilized to achieve the 50 m altitude (Figure 5.3). This path consists of 5 1/2 complete passes over the field at height increments of 8 m each. The launch height is assumed to be 2 m. In ideal flight conditions the time required to reach the 50 m altitude is approximately five minutes. The program which was utilized to determine the climb rates is in Appendix D.

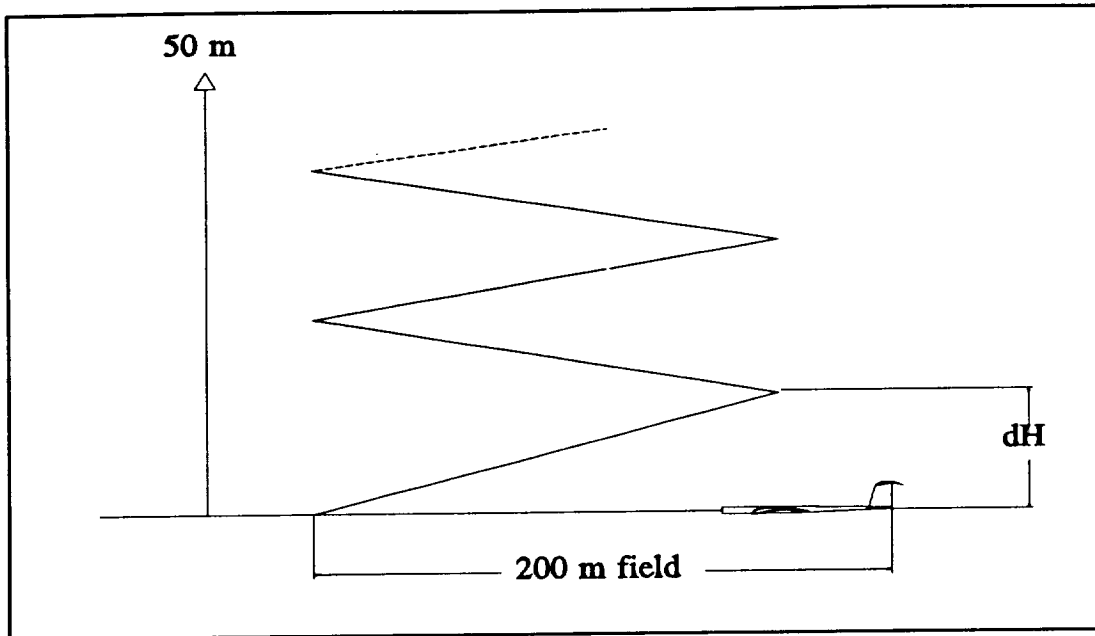


Figure 5.3 Proposed climb scheme

5.3 Banking and Turning

Another part of the plane's mission is to follow a "figure 8" flight pattern at the required altitude. In each "loop" of the "8" the plane flies a circular flight path determined by the turn radius. In order to turn, the plane must also bank towards the inside of the circle. Two forces must be taken into account: the centrifugal force and its opposing force, the $L\sin\alpha$ component (Figure 5.4). These forces must be in equilibrium for a steady turn. The turn radius and the banking angle are directly related, and their relationship is represented by equation 5.3:

$$R = \frac{(W/a)V^2}{L} \sin\alpha \quad [5.3]$$

where R is the turn radius, a is gravity, and α is the banking angle.

Substituting the values of weight with its lift component, equation 5.3 can be rewritten as equation 5.4.

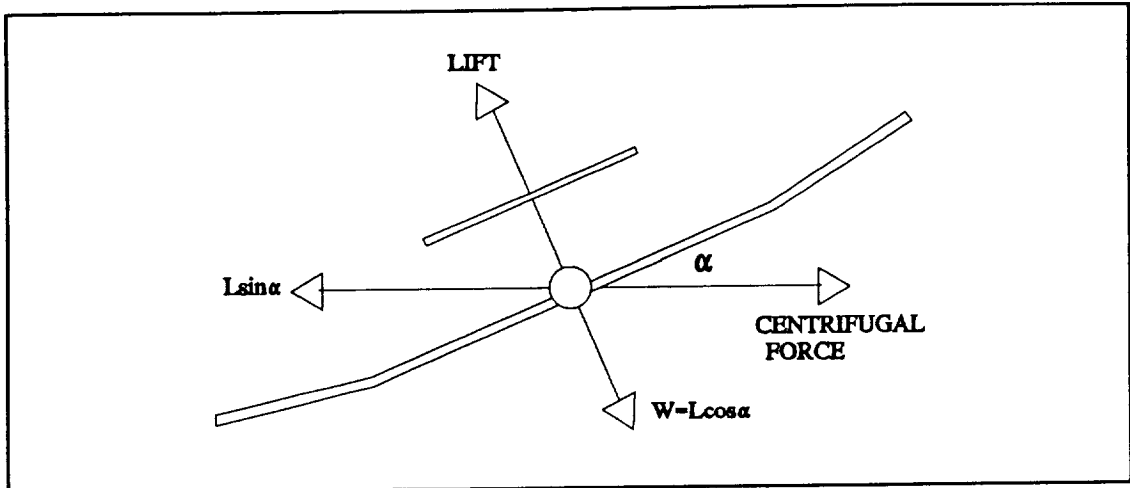


Figure 5.4 Frontal view of plane during turn

$$R = \frac{V^2}{g \tan \alpha} \quad [5.4]$$

Since the banking angles are small, the chosen angles of turn were iteratively determined to be between 3 deg. and 4 deg. These angles yielded turn radii of 89 m and 67 m, respectively. These values fit within our climb scheme and field of operation. The program developed to calculate the banking angle and the turn radius is also found in Appendix D.

CHAPTER 6
SOLAR CELLS AND ARRAY

6.1 Power Requirements and Design Parameters

The power requirements for level flight are met through the utilization of silicon solar cells. The level flight speed of 7 m/s and the weight of 52 Newtons dictate a minimum power requirement of 18.8 Watts. The solar array implemented on the plane produces approximately 108 Watts for the test flight date (April 11, 1992). This power production is calculated with the plane flying away from the sun thus exposing the greatest cell area to the sun's rays. The power produced for the plane flying toward the sun is approximately 98 Watts. These values do not include the power losses suffered in the motor/propeller transmission since even an optimized power train reduces the power by more than half.

A number of parameters control the amount of power produced as well as the construction of the array. The weight of the cells are considerable and compose a large portion of the overall weight of the plane. Therefore, the cells must produce more power to the overall thrust than they contribute to weight. Another consideration is the efficiency of the photovoltaic cells. The cells are rated at an efficiency of 12.5%. This value is determined at ideal conditions in a laboratory. The actual efficiency is lower due to nonideal real world conditions. The power loss due to poor impedance matching to the motor and losses from the resistance of the wiring is substantial. The geometry of the wing is also an important parameter. The wing section allows only a limited number of possible array configurations which limits the number of possible voltage-current options.

6.2 Photovoltaics and Solar Power

6.2.1 Photovoltaic Theory

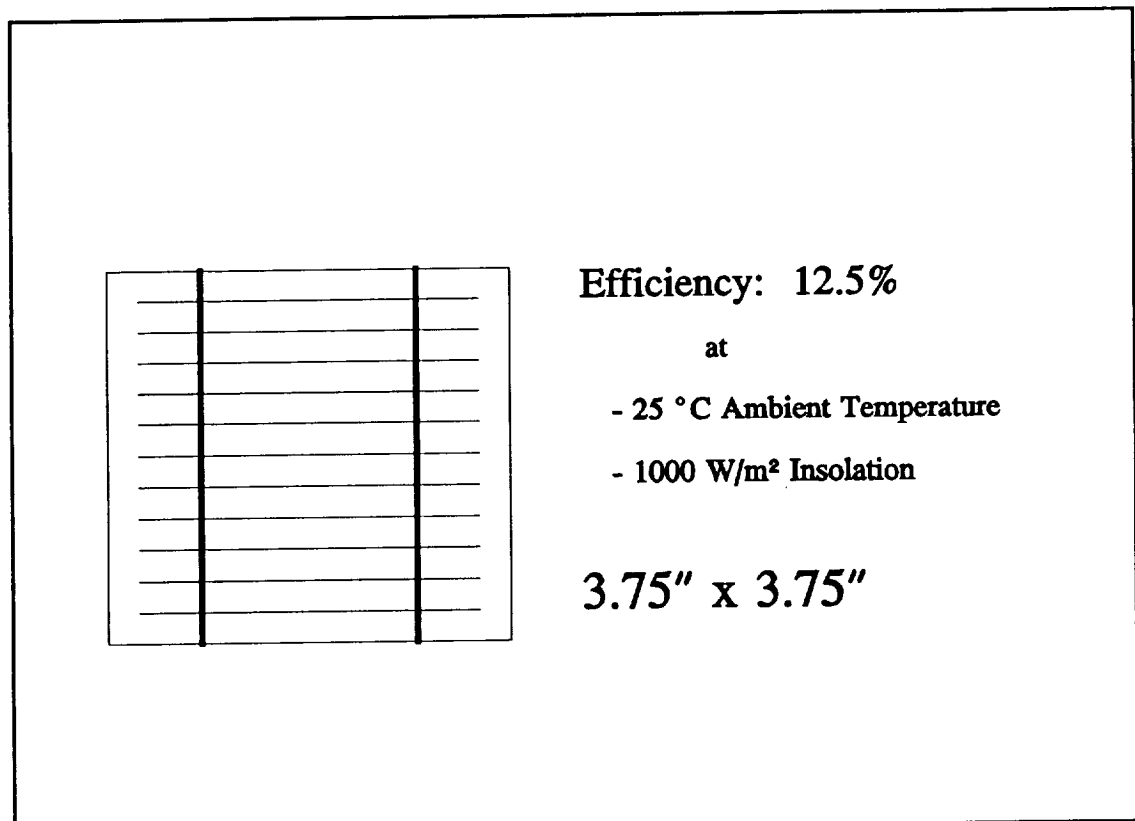


Figure 6.1 Mobil Solar Silicon Photovoltaic Cell.

A basic solar cell (Figure 6.1) consists of two layers of Silicon glass. The top layer is doped with Phosphorous to produce an excess of electrons while the bottom layer is doped with Aluminum to produce an abundance of electron holes. As photons strike the surface of the cell, they knock loose the excess electrons in the SiP bond. The net effect is the creation of free conduction electrons and positively charged holes which generate an electric potential between the top and bottom layers. Basic inefficiencies in

this process are reflection and recombination of the photons striking the cell. Also, some photons do not possess the energy to knock loose the electrons thus rendering some of the incident light ineffective. Other photons possess too much energy and waste the excess when striking the electrons. (Hu and White, 1983)

6.2.2 Solar Power Estimation¹

The amount of solar power reaching the cells on a given day relies on many geometric and atmospheric variables. Obviously, a clear sunny day is better than an overcast day, but summer months are not necessarily better than winter. Air pollution and building reflection contribute to the overall power availability. However, the position of the sun relative to the cells is the most dominant factor.

To find the estimated power available, the first step is to determine the day of the year. For this discussion, the day of the year stems from its numerical position from January 1st (e.g. January 2nd = 2, while December 30th = 364). In order to find the sun's position in the sky relative to the Earth, calculations to find the solar time must be performed: (Duffie and Beckman, 1980)

$$Q = \frac{360 \times (n - 81)}{364} \quad [6.1]$$

where n is the day of the year, and Q is a time variable. This value is now used to produce E, the equation of time variable:

¹A program utilizing the following equations to find the power generated by a solar array can be found in Appendix E.1.

$$E = 9.87 \times \sin(2 \times Q) - 7.53 \times \cos(Q) - 1.5 \times \sin(Q) \quad [6.2]$$

This variable, along with the local and standard meridians, adjusts the standard time to actual solar time:

$$\text{solar time} = \text{standard time} + 4(L_{st} - L_{loc}) + E \quad [6.3]$$

L_{loc} is the local meridian (for Worcester $L_{loc} = 71.805^\circ$), and L_{st} is the relative standard meridian for this section of the country ($L_{st} = 75^\circ$). The standard time is Eastern Standard Time and during daylight savings time, one hour must be added to find the solar time (e.g. if on April 30, solar noon is found to be 12:30 EST, it is actually at 1:30). Once the solar time is found, the geometric parameters for the sun's position may be calculated. The solar time is applied to find the hour angle, ω , the position of the sun east or west of the local meridian: (Duffie and Beckman, 1980)

$$\omega = \text{solar time} \times 15/60 \quad [6.4]$$

Solar noon occurs when the hour angle becomes 0. The maximum amount of power delivered to a solar array will be at this point (Figure 6.2).

The declination angle is defined as the angle between the equator and the sun's position at solar noon. For northern hemisphere calculations, the declination will be positive:

$$\delta = 23.45 \sin\left(\frac{360(284+n)}{365}\right) \quad [6.5]$$

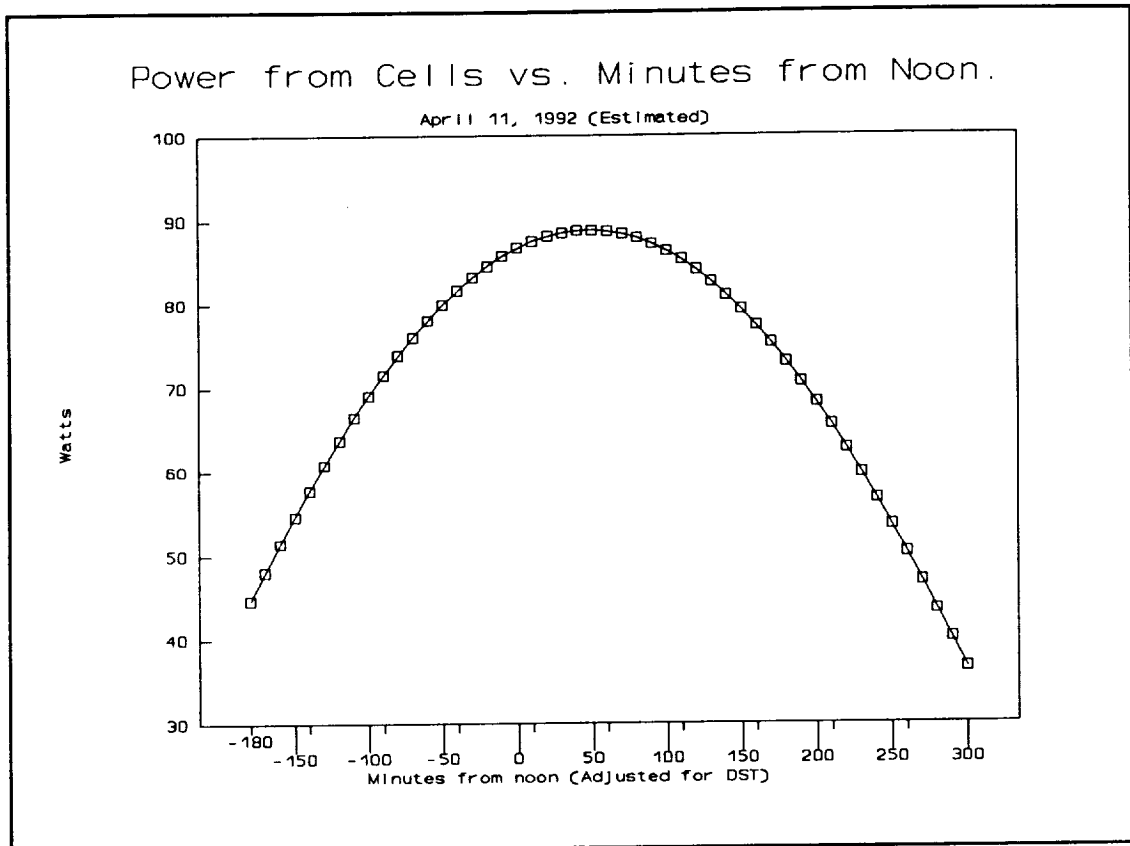


Figure 6.2 Graph of Power Produced by Cells vs. Time of Day.

The rest of the geometric angles are measured and are defined as:

ϕ is the latitude of the cell. (Worcester = 42.26°)

β is the slope of the cell relative to the ground. (see Figure 6.3)

γ is the surface azimuth angle and measures the east-west angle relative to line on the ground pointed to the sun.

θ is the angle of incidence which is the absolute angle of the sun's beam radiance and a line normal to the cell.

The angle of incidence relates to these various angles as in equation 6.6.

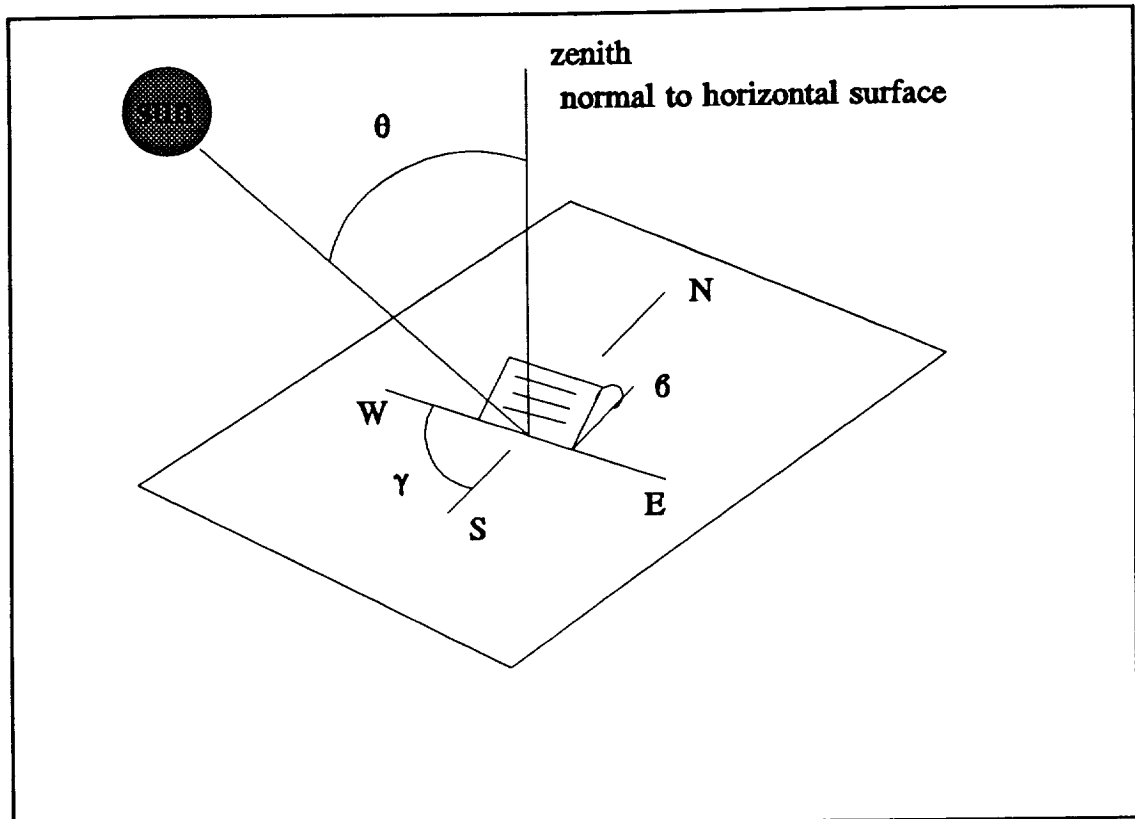


Figure 6.3 Sun Position Angles for Power Calculation.

$$\begin{aligned}
 \cos\theta &= \sin\delta\sin\phi\cos\beta - \sin\delta\cos\phi\sin\beta\cos\gamma \\
 &+ \cos\delta\cos\phi\cos\beta\cos\omega + \cos\delta\sin\phi\sin\beta\cos\gamma\cos\omega \\
 &+ \cos\delta\sin\beta\sin\gamma\sin\omega
 \end{aligned}
 \tag{6.6}$$

(Duffie and Beckman, 1980)

Although this equation is rather long and cumbersome, it may be simplified by setting the hour angle to zero. This will set the value of $\sin(\omega)$ to zero and force the last term to drop out. To simplify the equation further, set angles such as the surface azimuth angle or the ground slope angle to 0° or 90° and consequently the sines and cosines to 1.

The second factor in the power estimation is the solar insolation striking the Earth's outer atmosphere. Since the Earth travels in an elliptical orbit around the sun, this value, known as the solar constant, varies with the day of the year. An average yearly value of this constant, G_{sc} , has been studied and recorded to be 1353 W/m^2 . To find the adjusted solar constant for a day of the year, G_n , it is related as:

$$G_n = G_{sc} \left(1 + 0.033 \cos \frac{360n}{365} \right) \quad [6.7]$$

(Duffie and Beckman, 1980)

Atmospheric transmissivity is the last factor in determining the power reaching a cell on the ground. However, this cannot be measured directly and must be estimated. The transmissivity depends upon many variables including air pollution, relative humidity, time of day, and altitude. A method is offered by Hottel to estimate the clear day irradiance (Duffie and Beckman, 1980, p. 62).

Using this method, the atmospheric transmissivity, τ_{atm} , becomes 63% for Worcester in winter/spring. This seems low but will be used to insure that the power estimations are not too high.

The total insolation striking an area on the ground can now be found:

$$G_g = G_n \tau_{atm} \cos(\theta) \quad [6.8]$$

(Duffie and Beckman, 1980)

The units of G_g are W/m^2 , therefore the power incident on the area is simply G_g multiplied by the area.

Any sort of covering above the cells will also affect the transmissivity, since some

light will be reflected from the covering. The amount reflected will depend upon the angle of incidence of the sun's rays. Detailed calculations are found to estimate this amount lost. (Duffie and Beckman, 1980)

In any medium, the incident sunlight will refract to a certain degree and leave at a different angle. This will also alter the power generation of the array. The angle of refraction is related to the incident angle through trigonometry:

$$\frac{m_1}{m_2} = \frac{\sin\theta_{refr}}{\sin\theta_{inc}} \quad [6.9]$$

where m_1 and m_2 are refraction coefficients. Further geometric expressions relate the two angles:

$$r_{\perp} = \frac{(\sin\theta_{refr} - \sin\theta_{inc})^2}{(\sin\theta_{refr} + \sin\theta_{inc})^2} \quad [6.10]$$

$$r_{\parallel} = \frac{(\tan\theta_{refr} - \tan\theta_{inc})^2}{(\tan\theta_{refr} + \tan\theta_{inc})^2} \quad [6.11]$$

$$\tau_r = 0.5 \left[\frac{(1-r_{\parallel})}{(1+r_{\parallel})} + \frac{(1-r_{\perp})}{(1+r_{\perp})} \right] \quad [6.12]$$

where τ_r is the reflective transmittance or the amount of light not reflected.

New variables are introduced: k , the extinction coefficient for the covering, and l , the covering thickness². These new variables are related to an absorption coefficient,

²For the Surya analysis, values of k , m_2 and l used were 105, 1.64, and 0.0001 m respectively.

τ_a :

$$\tau_a = e^{\frac{-k l}{\cos\theta_{ref}}} \quad [6.13]$$

Finally, the covering transmissivity is a combination of the absorption and reflection:

$$\tau_{covering} = \tau_a \tau_r \quad [6.14]$$

6.2.3 Final Array Size

The power arriving is not the usable available energy, since the cells can only convert around 12.5% to electric power. This electric power will eventually be transformed into thrust for the aircraft through the motor and propeller combination. Therefore, the cells must produce enough power to overcome the losses induced by the power train to sustain level flight. Assuming that the power train will convert only about 20 to 30 %, this target and the estimated power produced dictate the initial number of cells to be installed upon the plane. With 18.8 Watts needed to fly the plane and the wing geometry in mind, the number of cells to be placed upon the wings is 120.

6.3 Array Construction

With the number of cells determined, an effective array must be constructed to produce a satisfactory combination of voltage and current. The motor operating voltage range is between 3.6 and 7.2 Volts with a current draw of 10 to 20 Amps depending

upon the speed of the propeller. These are the ranges that the cell array must fall within in order for the motor and propeller to produce thrust.

6.3.1 Solar Testing

The only way to know what each cell is producing is to take a random sampling of cells and test them in clear sunlight conditions. A small number of cells were taken to the roof of Salisbury Laboratories on the 18th of November 1991, and tested for their open circuit voltage and short circuit current. On that day, the individual cells produced approximately 0.5 Volts and, depending upon the orientation, 0.6 - 1.1 Amps. Another test was performed on February 6, 1992. This test used a ten cell array and sought the

characteristic I-V curve and maximum power point for the array. The I-V curve is a simple plot of the current vs. voltage and shows the

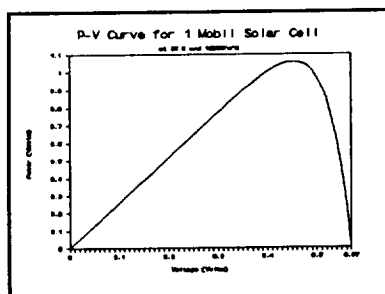


Figure 6.5 Typical P-V Curve for Solar Cell.

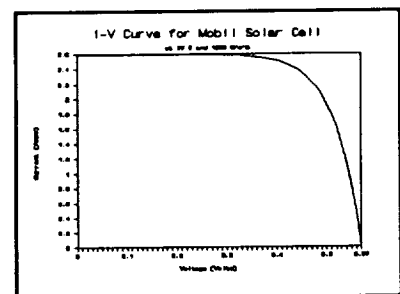


Figure 6.4 Typical I-V Curve for Solar Cell.

behavior of the cell under loads ranging from no resistance (short circuit) to infinite resistance (open circuit).

(Figures 6.4 and 6.6)

The maximum power point displays the voltage point that will produce the maximum

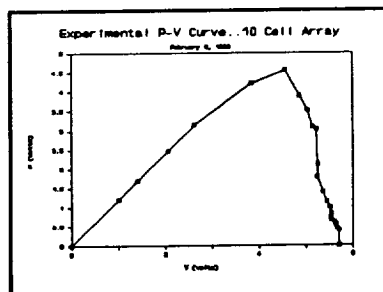


Figure 6.7 Experimental Results of 10 Cell Array.

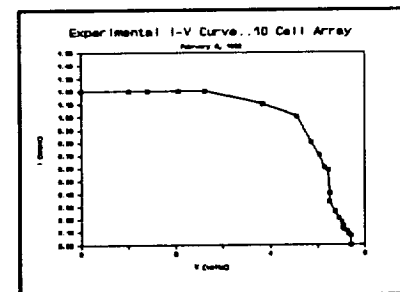


Figure 6.6 Experimental Results of 10 Cell Array.

amount of power. This is the target point when optimizing any load for the array.

(Figures 6.5 and 6.7) A table of values for the test are in Appendix E.2.

6.3.2 Cell Behavior

The voltage produced by a solar cell does not vary significantly with the light intensity except under very dim light conditions such as under fluorescent lighting. The current, however, depends entirely upon the intensity. Because of this, a clear cover on an array reduces the amount of current produced. With this knowledge, it was decided to place as many cells as possible on the outside of the wing to maximize power production. The fact that the voltage does not vary with light intensity prevents internal circuits from forming within the array. An internal circuit forms when one array in parallel with another has a significantly higher voltage and tries to force current through the lower array. This results in a net power loss and needs to be avoided. Placing arrays in parallel that do not have equal numbers of cells in series will also produce this internal circuit (e.g. an eleven cell array in parallel with a nine cell array). This is caused by the fact that electric potentials sum in series while currents sum in parallel. Consequently, each array on the plane must have an equal number of cells.

Another limitation of cells is that arrays at different inclination angles cannot be added in series. The reason for this is the different currents produced. An array directly facing the sun will create a current flow much higher than an array near parallel to the sun's rays. Although they will produce a higher voltage potential due to the additive property of cells in series, the current output will be the result of the weakest cell. An effective analogy would be the weak link in the chain. The current is only as powerful as the weakest cell. If these cells are connected, the higher current one will try to force current through the weaker and reverse voltage situations with possible cell destruction

may result. One shaded cell in series will also cause this effect.

Silicon solar cells are extremely brittle and fragile. Therefore, great care should be exercised when handling them. Fortunately, they can withstand short circuiting as well as extreme heat with no ill effects. Another trait of cells is their tendency to become very warm when in contact with sunlight. Depending upon the intensity, they may heat up to temperatures 50°C above ambient conditions.

6.3.3 Array Layout

The configuration of the array is based upon factors ranging from the geometry of the wing to the predicted load. The width of the wing allows for three rows of cells running the entire length of the top. The wing length was determined from the lift to drag ratio as well as the number of cells needed to power the plane. Due to airfoil integrity reasons, the first row on the leading edge is placed underneath the wing skin. The last two rows, because of power improvements, are placed on the outside of the wing on the rear of the airfoil.

The arrays should be angled to receive the greatest amount of sunlight at any given time. On a stationary platform the array would be angled at about 45° to the horizontal. Since the plane is constantly moving in the horizontal and vertical planes, the best inclination is to place them close to the horizontal. The front cells are inside facing forward and placed as close to horizontal as the wing geometry will allow at an angle of 12° to the chordline. The rear cells are subject to geometric constraints as well and are placed directly onto the flatback airfoil at angles of approximately 6° to the chordline.

The motors that had been expected for use all possessed operating ranges of 3.6

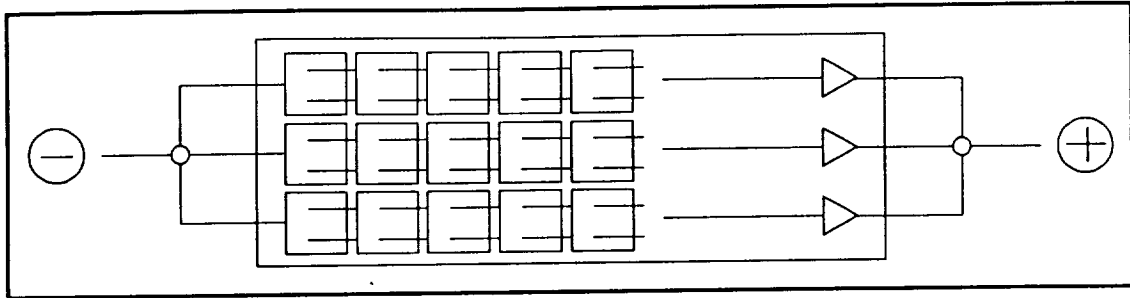


Figure 6.8 Modular Section of Wing Showing Cell Placement.

to 7.2 volts with 7.2 being the most efficient while the currents drawn climb to 20 amps for best efficiency. Since each row contains 40 cells, this is the maximum number of cells that may be connected in one string due to the inability to connect different rows. With 40 cells per row, the possible combinations must be divisors of that number. Therefore, the array strings may possess 1,2,4,5,8,10,20 or 40 cells. One through five will not develop enough voltage. 40 and 20 won't generate the required current to operate a motor. This leaves eight or ten. While eight cells will generate the right voltage, it is only slightly more than the minimum allowed. Therefore, ten cells is the best option for powering the motor.

The final array consists of twelve sub-arrays of ten cells. Each section of the wing (main and modular) bears three rows. (see Figure 6.8) All twelve are connected in parallel to generate an anticipated five volts and twelve amps according to the first test.

6.3.4 Array Construction

The entire array was constructed entirely by hand. Each of the 120 cells donated by Mobil Solar arrived naked. Two metal ribbon leads needed to be soldered to one side of every cell. This was accomplished with a small soldering iron and 60/40 lead/tin

solder. Once completed, ten unit arrays were assembled by soldering the leads of one cell to the back of another in a long chain. To integrate the cells to the wing created a slight problem. The front row could be easily placed upon small styrofoam shelves underneath the coating of plastic, but the back rows needed some way to adhere directly to the covering. Fortunately, a roll of double-sided adhesive was donated by Flexcon Corporation. This adhesive was applied in two half-inch strips to the backside upon which the array rested. To prevent disintegration of this bond and the cells, a small strip of plastic ran along the leading edge of the array and joined the wing approximately 1.5 inches in front of the cells. This prevented the airstream from finding its way underneath the cells and ripping them off.

CHAPTER 7
PROPULSION AND ELECTRONICS

7.1 Propulsion

7.1.1 Motor

The motor used to turn the propeller is the Astro-Cobalt 25. It is designed to operate with voltages from 3.6 to 7.2 Volts. The current draw of the motor depends upon the load, in this case the propeller. The motor was chosen only on its ability to operate within the voltage range of the array output. Efficiencies for this particular motor were not found for the applied input power.

7.1.2 Propeller

A 13"x7 propeller produces the thrust to fly the plane. The propeller is collapsible to reduce drag during unpowered flight. It also helps during landing as the collapsible prop will tend not to break off as easily as a fixed propeller. The propeller was selected through dead-air tests on a thrust/torque strain stand. The stand uses two small strain gauges to measure the produced torque and thrust for a given voltage and current. The propeller chosen produced the most thrust for available voltage-current values of 5 V and 14 A.

7.2 Electronics

7.2.1 Backup Batteries and Power Switch

In case of catastrophic failure, there is a small reserve battery pack installed in the fuselage of the plane. It is a package of seven 1.2 Volt rechargeable battery cells.

At full power they produce eight to nine volts and upwards of 20 amps. The use of these batteries is limited as their lifespan is not more than five or six minutes. There is a manual switch, run by an available servo, that is capable of switching the power source from the cells to the batteries. The batteries can be slowly recharged up to five volts during glides if the motor is turned off. A diode connected between the cells and the batteries prevents the batteries from charging the array.

7.2.2 Controls Wiring

Each control surface on the plane is operated by remote control through the use of small motors called servos. A very small current is needed to run them and each is controlled by its own channel frequency. Both ailerons are wired into the same channel to act in opposite directions. In other words, when one side is raised, the other will drop. The rudder and the horizontal stabilizer are wired separately and receive their own channels. All servos are wired to the receiver box where they pick up the signals for operation. The receiver itself needs a small battery pack to operate. These are four rechargeable 1.2 volt cells. There are enough channels available on the receiver to not only handle the control surfaces, but also the throttle and the main power switch. Figure 7.1 indicates the wiring diagram for the plane.

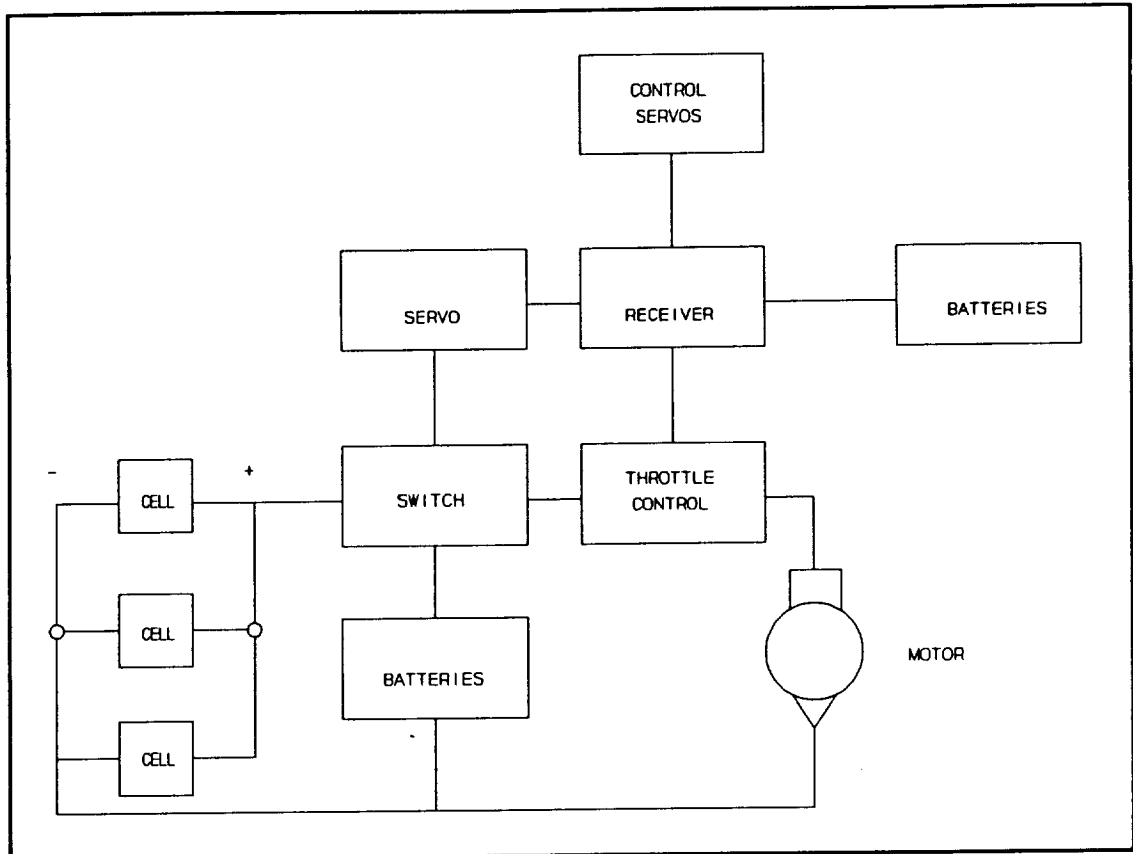


Figure 7.1 Schematic Showing Plane Wiring System.

CHAPTER 8
FLIGHT RESULTS

Surya underwent four flight tests between February and April of 1992. These tests proved not only to be valuable tools in the final design modifications but also as evidence of the sturdiness of the carbon composite structure. Due to the fragility of the solar cells, the first three test flights were completed before the cells were mounted. However, weights were used in place of the solar cells to estimate the behavior of the plane. The first flight test was without propulsion to verify that the location of the center of gravity was the same as that calculated theoretically. In this test, a slight wing twist was detected by the pilot, as well as a shift of the center of gravity from the desired location.

An overcorrected wing twist as well as another shift in the center of gravity persisted in the first powered flight test. The wing twist, now in the opposing direction, was again detected by the pilot. After adjustments were made to correct this by repositioning the modular wing sections, the plane proved to be responsive to controls and relatively easy to maneuver. The second power flight test utilized the propeller's full power, and the need to optimize the propulsion system with a more efficient motor and propeller became evident. Again, the plane responded well to controls and flew for a short amount of time before landing quietly on simple yet effective landing skids.

In the fourth test flight, proxy cell weights were replaced by the actual solar cells. The wing twist was corrected as attested by the pilot. However, the new electronic components installed for the wiring of the cells, shifted the center of gravity once again. This center of gravity shift and the presence of wind gusts caused the climb performance to be sluggish.

CHAPTER 9
CONCLUSION AND RECOMMENDATIONS

Many engineering difficulties were incurred during the design and construction of the solar plane, *Surya*. After the plane construction was completed, there appeared to be many components and processes which could be further optimized through more research, development and testing. Of course many of these revelations were not obvious to the project team before the actual construction began. The performance of *Surya* depends upon the following criteria: overall efficiency of the propulsion system, structural design, material selection, stability, aerodynamic analysis and the overall weight of the plane.

The efficiency of the propulsion system is determined by its individual components including the solar cells, wiring, motor, propeller and the electronic configurations. It is obvious that the propulsion system is limited by the 12.5% efficient solar cells but the system could be further optimized through better matching of the motor and propeller. The project team felt that a more efficient motor along with a more powerful propeller would further optimize the propulsion system. Unfortunately, due to time constraints the project team was unable to undertake this task. The project team also decided that to aid in the conservation of the weight budget, that a lighter wire could be used in the solar cell configuration.

The project team experienced difficulties in maintaining the stability of the plane. The center of gravity was not easy to maintain at one tenth of the chord length. The majority of the stability problems, encountered after *Surya* was completed could be eliminated by making the propulsion configuration a pusher propeller. This configuration would enable the center of gravity to be kept ahead of the main wing, even if cells were

placed on the horizontal stabilizer. In addition to increased stability, the pusher propeller configuration would allow an increase in the number of solar cells placed on the plane and allow for an increase in the power acquired from the cells.

Though *Surya* is structurally sound, the weight of the plane could greatly be reduced in most of the structural components. The handmade carbon composite fuselage and the wing and tail spars could be constructed more exactly to fully optimize the weight. The diameter of the fuselage could be reduced to conserve the weight of the plane. The diameter of the fuselage was originally dictated by a linkage used in the electronics. This linkage was later redesigned so that the fuselage diameter could be reduced. Many processes requiring the application of glue were done using epoxy, which tended to be heavier than standard superglue. The project team also felt that using the glue more sparingly would aid in the minimization of the weight of the plane.

The large size of the plane required that the wing sections of *Surya* be modular. The modular connections of the wing were constructed using a foam and carbon composite combination. These connections could be further optimized to conserve weight and possibly increase stability.

The control surfaces of the plane were increased in size to account for the increase in the size of the entire plane. After completion the plane seemed to be harder to control than had been anticipated. Enlarging the size of the control surfaces would aid in the overall performance of the plane.

Overall the project team was very satisfied with the analysis, design, construction and performance of *Surya*. The recommendations mentioned above indicate areas in which the project team felt limited. Most of these recommendations occurred at the completion of the plane and were realized through experience. Further research and

development in these areas are encouraged because the possibilities for various design configurations of this type of aircraft are numerous.

REFERENCES

Ault, H.K. & Scott, K.E., *WPI CAD LAB IPI Manual of Units*, Worcester Polytechnic Institute, (Worcester MA), 1991.

Baker, A. & Hoskin, B., *Composite Materials for Aircraft Structures*, American Institute of Aeronautics and Astronautics, Inc., (New York NY), 1986.

Beer, F.P., Johnston, E.R., *Mechanics of Materials*, McGraw Hill Book Company, (New York, NY), 1981.

Buresch, M., *Photovoltaic Energy Systems*, McGraw Hill Book Company, (New York NY), 1983.

Duffie, J.A. and Beckman, W.A., *Solar Engineering of Thermal Processes*, John-Wiley and Sons, (New York NY), 1980.

Hu, C. and White, R.M., *Solar Cells From Basic to Advanced Systems*, McGraw Hill Book Company, (New York NY), 1983.

Komp, R.J., *Practical Photovoltaics*, Aetec Publications, (Ann Arbor MI), 1981.

Kuethe, A. & Chow, C., *Foundations of Aerodynamics, 4th Ed.*, John-Wiley and Sons, (New York NY), 1986.

Lissaman, P., "Low-Reynolds Number Airfoils," *Annual Review of Fluid Mechanics Vol. 15*

Nikolai, L.M., *Fundamentals of Aircraft Design*, University of Dayton, (Dayton OH), 1975.

Norton, R.L., *Design of Machinery*, McGraw Hill Book Company, (New York NY), 1991.

Rauschenbach, H.S., *Solar Cell Array Design Handbook*, Van Nostrand Reinhold Company, (New York NY), 1980.

Raymer, D., *Aircraft Design: A Conceptual Approach*, AIAA, Inc., (Washington, DC), 1989.

Shevell, R.S., *Fundamentals of Flight*, Prentice Hall, (Englewood Cliffs NJ), 1989.

White, F., *Fluid Mechanics*, McGraw Hill Book Company, (New York NY), 1986.

APPENDICES

APPENDIX A

A.1 Glauert Method

In our analysis, the finite lift and drag coefficients of the wing and the tail are determined by using a Fourier-Series representation developed by Glauert (1937). In general, for any wing with symmetrical circulation distribution, the absolute angle of attack along the wing span can be express as the following:

$$\alpha_a(\theta) = \frac{m_{0_s} c_s}{m_0 c} \sum_{n=1}^{\infty} A_n \sin(n\theta) + \frac{m_{0_s} c_s}{4b} \sum_{n=1}^{\infty} n A_n \frac{\sin(n\theta)}{\sin\theta} \quad [\text{A.1}]$$

where the A_n terms represent the Glauert Constants. m is the sectional lift curve slope, c is the sectional chordlength, and b is the wing span. The subscript 's' refers to the sectional characteristics at the plane of symmetry. However, θ is a trigonometric representation for the position along the wing span.

After evaluating the Glauert constants, the finite lift and induced drag coefficients are found through the following relationships, respectively:

$$C_L = \frac{m_{0_s} c_s \pi b}{4S} A_1 \quad [\text{A.2}]$$

and

$$C_{D_i} = (C_{D_i})_{el} (1 + \sigma) \quad [\text{A.3}]$$

where:

$$\sigma = \sum_{n=2}^{\infty} \left(\frac{nA_n^2}{A_1^2} \right) \quad [\text{A.4}]$$

$$(C_D)_{el} = \frac{C_L^2}{\pi AR} \quad [\text{A.5}]$$

In addition, a computer program was used to solve the Glauert constants, the finite lift coefficient and the induced drag coefficient for any untwisted rectangular wing. The program was written in Pascal as follows:

```

program finite (input, output);

var
  z1, z          : array [1..10, 1..10] of real;
  mw, bw, cw, ARw, Sw, CLw, CDi  : real;
  A1, A3, A5, A7  : real;
  Abs_attack_angle_w : real;
  mu, pi, density, sigma      : real;

function power (x, n : real): real;

var
  temp : real;

begin
  temp:= exp(n*ln(x));
  power:= temp;
end;

```

```
procedure glauert (var AR, m      ; real;
                  var g1, g3 g5, g7, abs_attack_angle : real);
```

```
var
  alpha1, alpha2, alpha3, alpha4 : real;
  i, j, l : integer;
  factor : real;
```

```
begin
```

```
  alpha1:= 3.141592654/8;
  alpha2:= 3.141592654/4;
  alpha3:= 3.141592654/8*3;
  alpha4:= 3.141592654/2;
```

```
  for j:= 1 to 7 do
```

```
    begin
```

```
      z1[1,j]:= sin(j*alpha1)*(1+j*m/4/sin(alpha1)/AR);
      z1[2,j]:= sin(j*alpha2)*(1+j*m/4/sin(alpha2)/AR);
      z1[3,j]:= sin(j*alpha3)*(1+j*m/4/sin(alpha3)/AR);
      z4[4,j]:= sin(j*alpha4)*(1+j*m/4/sin(alpha4)/AR);
```

```
    end;
```

```
  for j= 1 to 4 do
```

```
    begin
```

```
      z[1,j]:= z1[1,(2*j-1)];
      z[2,j]:= z1[2,(2*j-1)];
      z[3,j]:= z1[3,(2*j-1)];
      z[4,j]:= z1[4,(2*j-1)];
```

```
    end;
```

```
  for i:= 1 to 4 do
```

```
    z[i,5]:= abs_attack_angle;
```

```
  for l:=1 to 3 do
```

```
    for i:= 1 to 3 do
```

```
      begin
```

```
        factor:= z[l,l]/z[i+1,l];
```

```
        for j:= 1 to 5 do
```

```
          z[i+1,j]:= z[l,j]-(z[i+1,j]*factor);
```

```
        end;
```

```
  g7:= (z[4,5]/z[4,4]);
```

```
  g5:= (z[3,5]-g7*z[3,4])/z[3,3];
```

```
  g3:= (z[2,5]-g7*z[2,4]-g5*z[2,3])/z[2,2];
```

```
  g1:= (z[1,5]-g7*z[1,4]-g5*z[1,3]-g3*z[1,2])/z[1,1];
```

```

end;

begin

  {sectional lift curve slope of wing } mw:= 5.17;
  {sectional chord length of wing    } cw:= 0.424;
  {span of wing                      } bw:= 4.5;
  {absolute attack angle at wing     } abs_attack_angle_w:= 0.191630;
  pi:= 3.141592654;
  density:= 1.225; {standard atmosphere at sea level}
  mu:= 1.7894E-5; {standard atmosphere at sea level}

  ARw:= bw/cw;
  glauert (ARw, mw, A1, A3, A5, A7, abs_attack_angle_w);
  Sw:= bw*cw;
  CLw:= mw*cw*pi*bw*A1/4/Sw;
  sigma:= (3*A3*A3+5*A5*A5+7*A7*A7)/A1/A1;
  CDi:= CLw*CLw/pi/ARw/(1/(1+sigma));

  writeln;
  writeln ('-----');
  writeln ('          results of calculation          ');
  writeln ('-----');
  writeln;
  writeln ('lift coefficient of wing           = ', CLw:12:8);
  writeln ('induced drag coefficient of wing       = ', CDi:12:8);
  writeln ('aspect ratio of wing                    = ', ARw:12:8);
  writeln ('deviation from elliptic wing            = ', sigma:12:8);

end.

```


APPENDIX B

B.1 Carbon Composite Testing

The following calculations were done after a strength test was performed on a sample carbon composite tube. The tube was placed in a vice and a force was gradually applied at the free end to simulate the forces applied to the wing. A total force of 114.48 Newtons was applied to the tube before fracture occurred. The force was applied at a distance of 0.40 m which created a moment of 45.792 N*m. This calculation is shown in the following equation.

$$M = F * d = (114.48N)(0.40m) = 45.792Nm \quad (B.1)$$

The inner diameter of the tube was 2.2225 cm or 0.02225 m. The thickness of the fabric was 0.01778 cm. The outer diameter of the tube was then calculated using the following:

$$d_o = d_i + 4(thickness) \quad (B.2)$$

The resulting outer diameter was 2.2936 cm or 0.022936 m. Using these diameters the moment of inertia was calculated.

$$I = \frac{\pi(d_o^4 - d_i^4)}{64} = 1.59 \times 10^{-9}m^4 \quad (B.3)$$

The stress that the tube endured was then calculated from the equation:

$$\sigma = \frac{(M)(c)}{I} \quad (B.4)$$

where c is equal to one half of the outer diameter or 0.01148 m. The maximum stress that a tube of this diameter with two layers of carbon composite fabric could withstand was calculated to be $3.303 \times 10^8 \text{ N/m}^2$.

TK SOLVER FILE - Wing Spar

*****RULE SHEET*****

S Rule

```

di = do - (2*#lay*fabth)
Irod = (PI)*((do^4)-(di^4))/64
Jrod = (PI)*((do^4)-(di^4))/32
Arod = (PI)*((do^2)-(di^2))/4
Vspar = Aspar*Swing
mspar = Vspar*Dcomp
Swing = Sprim + (2*Smod)
w = Lwing/Swing
Mdisprim = ((w*(.5*Sprim)^2)/2)
Mmod = (w*Smod^2)/2
Mmaxprim = Mdisprim + Mmod
Sapp = (Mmaxprim*(.5*do))/Irod
SF = Sallow/Sapp
    
```

*****VARIABLE SHEET*****

St	Input	Name	Output	Unit
	4.50	Swing		m
	144.9	Lwing		N
		w	32.2	N/m
	.0201	do		m
		di	.01907925	m
		Arod	.00003141	m^2
		Vspar	.00014134	m^3
	1089	Dcomp		kg/m^3
		mspar	.15392409	kg
		Irod	1.5077E-9	m^4
		Jrod	3.0155E-9	m^4
		Mmaxprim	41.25625	N*m
	2.5	Sprim		m
		Mmod	16.1	N*m
	1.0	Smod		m
		Sapp	2.75E8	N/m^2
	1.2	SF		
		Mdisprim	25.15625	N*m
G		#lay	3.000221	
	.0001778	fabth		m
	3.30E8	Sallow		N/m^2

TK SOLVER FILE - Tail Spar

*****RULE SHEET*****

S Rule

```

di = do - (2*th)
th = (lay#)*(fabth)
Irod = (PI()*((do^4)-(di^4)))/64
Jrod = (PI()*((do^4)-(di^4)))/32
Arod = (PI()*((do^2)-(di^2)))/4
Vspar = Aspar*Stail
mspar = Vspar*Dcomp
wtail = Ltail/Stail
Mmaxtail = (wtail*(.5*Stail)^2)/2
Sapp = (Mmaxtail*(.5*do))/Irod
SF = Sallow/Sapp
    
```

*****VARIABLE SHEET*****

St	Input	Name	Output	Unit
	1.0	Stail		m
	144.9	Ltail		N
		wtail	11.1	N/m
		do	.01376680	m
	.0127	di		m
		Arod	2.1181E-5	m^2
		Vspar	2.1181E-5	m^3
	1089	Dcomp		kg/m^3
		mspar	.02306658	kg
		Irod	4.627E-10	m^4
		Jrod	9.255E-10	m^4
		Mmaxtail	18.549329	N*m
		Sapp	2.75E8	N/m^2
	1.2	SF		
G		#lay	3.000221	
	.0001778	fabth		m
	3.30E8	Sallow		N/m^2

APPENDIX C

```

1 CLS
10 REM
19 REM          STABILITY ANALYSIS      with inputs
20 REM
21 REM          THIS PROGRAM WILL CALCULATE THE POINT OF NEUTRAL STABILITY
22 REM          (dCM/dCL = 0), AND THE OVERALL STABILITY OF A SIMPLE AIRCRAFT
23 REM          ASSUMING THE WING AND TAIL ARE OF THE SAME AIRFOIL SECTION.
24 REM          FOR THIS PROGRAM YOU MUST INPUT WING AND TAIL d(CL)/d(ALPHA)
30 REM
40 REM
50 REM -----VARIABLES-----
51 REM
60 REM          NU = TAIL EFFICIENCY FACTOR
70 REM          SH = HORIZONTAL TAIL PLANFORM AREA
80 REM          SW = WING PLANFORM AREA
85 REM          SRAT = SH/SW
90 REM          E = dE/da (.45 for low tail, .1 for high tail)
100 REM         LH = DISTANCE FROM WING AERODYNAMIC CENTER TO HORZ. STAB.
110 REM         FUS = dCM/dCL FOR THE FUSELAGE ( 0 for simple model )
120 REM         C = CHORD LENGTH
130 REM         X = DIST. FROM WING AERO CTR TO CTR OF GRAVITY
140 REM         NEUTPT = POINT OF NEUTRAL STABILITY
150 REM         STABIL = STABILITY OF CONFIGURATION ( < 0 IS STABLE)
160 REM
170 REM -----INPUTS-----
171 REM
180 INPUT " TAIL EFFICIENCY FACTOR (NU)          ";NU
190 INPUT " HORZ. STABILIZER PLANFORM AREA (m^2) ";SH
192 INPUT " HORZ. STABILIZER SPAN LENGTH (m)     ";BH
200 INPUT " WING PLANFORM AREA (m^2)           ";SW
202 INPUT " WING SPAN LENGTH (m)                ";BW
210 INPUT " d(DOWNWASH)/d(ALPHA)                ";E
212 INPUT " WING LIFT CURVE SLOPE (1/RAD)";DCLDAW
213 INPUT "TAIL LIFT CURVE SLOPE (1/RAD)";DCLDAH
220 INPUT " DIST, WING A.C. TO HOR STAB. (m) ";LH
230 INPUT " FUSELAGE EFFECT ON STABILITY      ";FUS
240 INPUT " WING CHORD LENGTH (m)            ";C
250 INPUT " DIST, C.G. TO WING A.C. (m)      ";X
269 REM
270 REM -----CALCULATIONS-----
275 REM
276 PI = 3.141593
280 SRAT = SH / SW
290 ARH = BH^2 / SH
300 ARW = BW^2 / SW
305 REM
330 REM
340 XXX = (1 - E) * SRAT * NU * (DCLDAH/DCLDAW)
350 REM
360 NP = (XXX * (LH/C) - FUS) / (1 + XXX)
370 NEUTPT = NP * C
375 REM
380 PRINT
390 PRINT " THE PT. OF NEUTRAL STABLITY IS LOCATED ";
400 PRINT USING "##.###";NEUTPT;
410 PRINT " m BEHIND THE WING A.C."
430 STABIL = (X/C) - NP
500 PRINT " dCM/dCL (stability) = ";
510 PRINT USING "##.###";STABIL;

```

APPENDIX D


```

10 REM
20 REM          MIN LEVEL FIGHT VELOCITY PROGRAM
30 REM-----
   REM SET VARIABLES
50 REM          WCL=Wing coeff of lift           W=weight of plane
60 REM          P=Density of air                 V=velocity
70 REM          SW=wing planform area           POW=power
80 REM          DP=parasitic drag coeff         B=wing span
90 REM          AR=aspect ratio                 E=airplane efficiency factor
100 REM-----
110 LPRINT "MINIMUM VELOCITY PROGRAM"
120 LPRINT
200 REM FORMULA: V=SQR(W/WCL*SW*P*0.5)
220 REM Wing is assumed to be the only liftig surface at min. level flight,
240 REM lift is approx. = weight
260 REM POWER = DRAG * VELOCITY
1000 REM-----
1100 LPRINT "Input variables"
1200          INPUT "          density of air(kg/m^3): ";P
1210          LPRINT "          density of air(kg/m^3): ";P
1300          INPUT "          weight of plane(N): ";W
1310          LPRINT "          weight of plane(N): ";W
1400          INPUT "          wing planform area(m^2): ";SW
1410          LPRINT "          wing planform area(m^2): ";SW
1450          INPUT "          wing span(m): ";B
1455          LPRINT "          wing span(m): ";B
1500          INPUT "          wing coeff. of lift: ";WCL
1550          LPRINT "          wing coeff. of lift: ";WCL
1600          INPUT "          wing parasitic drag coeff: ";DP
1610          LPRINT "          wing parasitic drag coeff: ";DP
1700          INPUT "          airplane efficiency factor: ";E
1710          LPRINT "          airplane efficiency factor: ";E
1900 LPRINT
2000          V=SQR(W*2/(WCL*SW*P))
2100 LPRINT "Min. level flight velocity (m/s): ";V
2150          AR=(B^2)/SW
2200          X=(WCL^2)/(3.1416*AR*E)
2300          POW=(V^3)*SW*.5*P*(DP+X)
2500          V=V*2.237
2600 LPRINT "          (mph): ";V
2700 LPRINT "power required (watts): ";POW
5000 END

```

```

10 REM
20 REM          CLIMB RATE PROG
30 REM
40 REM  Set variables
50 REM          W = weight of plane
60 REM          PA = power available
70 REM          POW = power required for level-flight
80 REM          DH = rate of climb
90 REM          S = excess power
-----
100 REM
200 PRINT "CLIMB RATE"
210 PRINT
220 PRINT "Input variables"
300          INPUT "          weight of plane(N): ";W
320          INPUT "          level-flight power required(watts): ";POW
350          INPUT "          power available(watts): ";PA
400 PRINT
700          LET S = PA-POW
710          LET DH = S/W
800          PRINT "Rate of climb: ";DH; "m/s"
2000 END

```

```

10 REM
20 REM          BANKING PROGRAM
25 REM-----
30 REM variables:      V=VELOCITY OF LEVEL FLIGHT
4   EM              r=turn radius
50 REM              phi=banking angle
60 REM              dummies =x,y
65 REM-----
70 REM formula used: r= (v^2)/g*tan phi
90 REM-----
100 PRINT "PLANE BANKING PROGRAM"
110 PRINT
120 PRINT "Program Choice:"
130 PRINT "Find:turn radius->given: angle & velocity, select 1"
140 PRINT "Find:banking angle->given: velocity & turn radius, select 2"
150 INPUT "SELECTION: ";X
160     IF X=1 THEN GOTO 1000
170     IF X=2 THEN GOTO 2000
180 GOTO 150
200 REM-----
1000 PRINT "Turn Radius"
1010 INPUT "Velocity (m/s): ";V
1020 INPUT "Banking angle (degrees): ";PHI
1025     LET PHI=PHI*(3.1416/180)
1030     LET R=(V^2)/(9.810001* TAN(PHI))
1035 PRINT
1040 PRINT "Turn Radius: ";R; "m"
1050 GOTO 3000
1900 REM-----
2000 PRINT "Banking Angle"
2010 INPUT "Velocity (m/s): ";V
2020 INPUT "Turning radius (m): ";R
2030     LET Y=(V^2)/(R*9.810001)
2040     LET PHI= ATN(Y)
2045 PRINT
2050 PRINT "Banking angle: ";PHI;"rad"
2060     LET PHI=PHI*(180/3.1416)
2070 PRINT "          : ";PHI;"deg"
3000 END

```

APPENDIX E

E.1 Array Power Program

The following program, written in the Pascal programming language, estimates the solar power generated by a solar array. The program requires the user to enter various position angles, time variables and the number of cells in the array. It is also capable of solving the power output for an array with a transparent cover if the refraction index, extinction coefficient and the thickness are known. A sample output for the array installed on Surya follows for the case of flying toward the sun.

Program cellpowr (input,output);

const

pi = 3.141592654;
celleff = 0.125;
airindex = 1;

var

n, Q, E : real;
lloc, standtim, hourdum : real;
hour, decl, dummy1 : real;
lat, dummy2, beta : real;
dummy3, gamma, numcell : real;
A, B, C : real;
D, F, incadum : real;
inca, solc, alt : real;
incazdum, incaz, k : real;
aone, azero, taub : real;
taud, transatm, index : real;
cover : integer;
benddum, bend, rpd : real;
rpl, taur, extc : real;
thik, taua, taucover : real;
pwrsqm, acells, cellpow : real;
powerout, soltime, fool : real;
angle, reflang : real;

begin

writeln('Enter the day of the year; Jan. 1 = 1, Dec. 31 = 365');
readln (n);
Q := ((360(n-81))/364)*pi/180;*
*E := 9.87*sin(2*Q) - 7.53*cos(Q) - 1.5*sin(Q);*
writeln('Enter local longitude; local standard = 75');
readln (lloc);
writeln('Enter time from 12:00 in minutes; AM is -, PM is +');
readln (standtim);
soltime := standtim + 4(75-lloc) + E;*

```

hourdum := (soltime/60)*15;
hour := hourdum*pi/180;
decl := 23.45*pi/180*sin(0.0172142*(284+n));
writeln('Enter latitude');
readln (dummy1);
lat := dummy1*pi/180;
writeln('Enter angle w/ respect to the ground of array');
readln (dummy2);
beta := dummy2*pi/180;
writeln('Enter angle w/ respect to plane of sun');
readln (dummy3);
gamma := dummy3*pi/180;
writeln('Enter # of cells in array');
readln (numcell);
A := sin(decl)*sin(lat)*cos(beta);
B := sin(decl)*cos(lat)*sin(beta)*cos(gamma);
C := cos(decl)*cos(lat)*cos(beta)*cos(hour);
D := cos(decl)*sin(lat)*sin(beta)*cos(gamma)*cos(hour);
F := cos(decl)*sin(beta)*sin(gamma)*sin(hour);
incadum := A - B + C + D + F;
solc := 1353*(1+0.033*cos(n*0.0172142));
writeln('Enter altitude in kilometers');
readln (alt);
incazdum := cos(decl)*cos(lat)*cos(hour) + sin(decl)*sin(lat);
incaz := arctan(sqrt((1-sqr(incazdum))/sqr(incazdum)));
k := (0.2311 + 0.01858*sqr(2.5-alt))*1.00;
aone := (0.5055 + 0.00595*sqr(6.5-alt))*1.01;
azero := (0.4237 - 0.00821*sqr(6-alt))*1.03;
taub := azero + aone*exp(-k/cos(incaz));
taud := 0.2710 - 0.2939*taub;
transatm := taub + taud;
writeln('Enter 1 for a transparent cover or 2 for direct sunlight');
readln (cover);
taucover := 0;
if cover = 1 then begin
    writeln('Enter cover refraction index');
    readln (index);
    benddum := sin(inca)*airindex/index;
    bend := arctan(sqrt(sqr(benddum)/(1-sqr(benddum))));
    rpd := sqr(sin(bend-inca))/sqr(sin(bend+inca));
    rpl := sqr(sin(bendinca)/cos(bendinca))/sqr(sin(bend+inca)/cos(bend+inca));
    taur := 0.5*((1-rpl)/(1+rpl)) + ((1-rpd)/(1+rpd));
    writeln('Enter extinction coefficient');
    readln (extc);
    writeln('Enter coating thickness in meters');
    readln (thik);
    taua := exp(-extc*thik/cos(bend));
    taucover := taua*taur;

```

```

    transatm := transatm*taucover
end;
angle := inca*180/pi;
writeln('The incident angle is equal to ',angle:5:5,' degrees. ');
if (incadum > 0) then begin
    pwrsqm := solc*transatm*cos(inca);
    acells := numcell*0.009073;
    cellpow := pwrsqm*acells
end
else cellpow := 0;
powerout := cellpow*celleff;
writeln('The power from the cells is ',powerout:5:5,' Watts');
writeln('The total transmissivity is ',transatm:5:5, '. ');
writeln('The total power reaching the cells is ',cellpow:5:5,' Watts');
writeln('The total cell area = ',acells:5:5,' sqr. meters. ');
reflang := bend*180/pi;
writeln('The transmissivity of the covering is ',taucover:5:5, '. ');
writeln('The refraction angle is ',reflang:5:5,' degrees. ');
writeln('Enter a number to return to program. ');
readln (fool)
end.

```

Enter the day of the year; Jan. 1 = 1, Dec. 31 = 365
102
Enter local longitude; local standard = 75
71.805
Enter time from 12:00 in minutes; AM is - , PM is +
0
Enter latitude
42.26
Enter angle w/ respect to ground of array
8
Enter angle w/ respect to plane of sun
0
Enter # of cells in array
40
Enter altitude in kilometers
0.19
Enter 1 for a transparent cover or 2 for direct sunlight
1
Enter coating refraction index
1.64
Enter extinction coefficient
105
Enter coating thickness in meters
0.0001

The incident angle is equal to 26.10668 degrees.
The power from the cells is 34.45285 Watts.
The total transmissivity is 0.62891.
The total power reaching the cells is 275.62278 Watts.
The total cell area = 0.36292 sqr. meters.
The transmissivity of the covering is 0.87809.
The refraction angle is 15.56429 degrees.
Enter a number to return to program.

Enter the day of the year; Jan. 1 = 1, Dec. 31 = 365
102
Enter local longitude; local standard = 75
71.805
Enter time from 12:00 in minutes; AM is - , PM is +
0
Enter latitude
42.26
Enter angle w/ respect to ground of array
10
Enter angle w/ respect to plane of sun
180
Enter # of cells in array
80
Enter altitude in kilometers
0.19
Enter 1 for a transparent cover or 2 for direct sunlight
2

The incident angle is equal to 44.03202 degrees.
The power from the cells is 62.82775 Watts.
The total transmissivity is 0.71622.
The total power reaching the cells is 502.62204 Watts.
The total cell area = 0.72584 sqr. meters.
The transmissivity of the covering is 0.00000.
The refraction angle is 15.56429 degrees.
Enter a number to return to program.

E.2 Cell Test

Results of 10 cell array test of February 6, 1992.

Resistance	Voltage	Current	Power
Short Circuit	0	1.2	0
0.5 (Ω)	1.01 (V)	1.2 (A)	1.212 (W)
1	1.41	1.2	1.692
1.5	2.06	1.2	2.472
2	2.62	1.2	3.144
3	3.84	1.1	4.224
4	4.56	1.0	4.56
5	4.86	0.8	3.888
6	5.03	0.7	3.521
7	5.14	0.6	3.084
10	5.25	0.4	2.1
15	5.24	0.34	1.78
20	5.36	0.26	1.39
25	5.44	0.21	1.142
30	5.51	0.18	0.992
35	5.54	0.15	0.831
40	5.53	0.13	0.719
45	5.54	0.12	0.665
50	5.6	0.11	0.616
55	5.64	0.1	0.564
60	5.64	0.09	0.508
65	5.66	0.08	0.453
70	5.7	0.07	0.399
Open Circuit	5.63	0	0

APPENDIX F

F.1 Fuselage Weight Budget

FUSELAGE	MASS(g)	% FUSELAGE
Carbon Composite Frame	900.0	48.9
Servo	21.5	1.2
Wiring	98.3	5.3
Motor	245.7	13.3
Nose cone	56.8	3.1
Propeller	42.9	2.3
Receiver Batteries	101.0	5.5
Receiver	44.0	2.4
On/Off Switch	63.3	3.4
Emergency Batteries	238.0	12.9
Miscellaneous	32.0	1.7
TOTAL	1843.5	100.0

F.2 Wing Weight Budget

WING	MASS(g)	% WING
Carbon Composite Spar	478.0	15.9
Ribs	132.0	4.4
Leading Edge	116.0	3.8
Trailing Edge	58.0	1.9
Ailerons	99.0	3.3
Spar Webs	44.8	1.5
Skin(Mylar)	254.5	8.4
Wing Tips	36.1	1.2
Solar Cells	1142.0	37.9
Servos	43.0	1.4
Wiring	148.0	4.9
Reinforced Ribbs	158.0	5.3
Modular Tubing Connection	107.0	3.6
Landing Gear	58.0	1.9
Miscellaneous	139.0	4.6
TOTAL	3013.4	100.0

F.3 Tail Weight Budget

TAIL	MASS(g)	% TAIL
Ribs	14.8	3.3
Leading Edge	25.8	5.7
Elevator	43.9	9.7
Spar Webs	6.4	1.4
Skin (Mylar)	47.3	10.5
Vertical Stabilizer	160.0	35.4
Servos	43.0	9.5
Carbon Composite Spar	59.0	13.0
Balsa Rudder	12.0	2.7
Miscellaneous	40.0	8.8
TOTAL	452.2	100.0

APPENDIX G

